Government of **Western Australia**
Department of **Mines, Industry Regulation and Safety**

RECORD 2019/9

APPLICATION OF RAPID BENCHTOP X-RAY POWDER DIFFRACTOMETRY FOR IDENTIFICATION AND CHARACTERIZATION OF MINERAL PHASES IN GEOLOGICAL MATERIALS

by

MJ Wawryk and EA Hancock

Geological Survey of Western Australia

Government of **Western Australia**
Department of **Mines, Industry Regulation and Safety**

RECORD 2019/9

APPLICATION OF RAPID BENCHTOP X-RAY POWDER DIFFRACTOMETRY FOR IDENTIFICATION AND CHARACTERIZATION OF MINERAL PHASES IN GEOLOGICAL MATERIALS

by
MJ Wawryk and EA Hancock

PERTH 2019

Geological Survey of Western Australia

REFERENCE
The recommended reference for this publication is:
Wawryk, MJ and Hancock, EA 2019, Application of rapid benchtop X-ray powder diffractometry for identification and characterization of mineral phases in geological materials: Geological Survey of Western Australia, Record 2019/9, 25p.

ISBN 978-1-74168-865-8
ISSN 2204-4345

Grid references in this publication refer to the Geocentric Datum of Australia 1994 (GDA94). Locations mentioned in the text are referenced using Map Grid Australia (MGA) coordinates, Zone 50. All locations are quoted to at least the nearest 100 m.

Published 2019 by the Geological Survey of Western Australia
This Record is published in digital format (PDF) and is available online at <www.dmp.wa.gov.au/GSWApublications>.

Further details of geoscience products and maps are available from:
Information Centre
Department of Mines, Industry Regulation and Safety
100 Plain Street
EAST PERTH WESTERN AUSTRALIA 6004
Telephone: +61 8 9222 3459 Facsimile: +61 8 9222 3444
www.dmp.wa.gov.au/GSWApublications

Cover image: Sunset over the Yalgoo Mineral Field. Photograph by T Ivanic, DMIRS

Contents

Abstract 1
Introduction 1
Fundamental principles of X-ray powder diffraction 1
    Powder diffraction patterns 2
    X-ray fluorescence 3
The benchtop X-ray diffractometer 4
    Instrument hardware 4
    Vibrating sample holder 5
    Detection limits 5
    Sample preparation and operation 6
Data and analysis 6
    Qualitative analysis 7
        Mineral phase identification 7
        Elemental identification 8
    Quantitative analysis 8
        Reference intensity ratio analysis 8
        Rietveld refinement 8
    Clay mineral identification 9
    CSIRO powdered standards 10
    Comparison with laboratory-based XRD 10
Applications of X-ray powder diffractometry 12
    Specimens from Greenbushes Li–Cs–Ta pegmatite 12
    Drillcore from the Corybas 1 well 16
Conclusion 18
References 20

Figures

1. Bragg's diffraction diagram 2
2. Diagram of Debye–Scherrer diffraction cones 2
3. Diagram of an X-ray diffraction pattern 3
4. Diagram of X-ray fluorescence 3
5. Example of an X-ray fluorescence pattern 4
6. The GSWA benchtop XRD with external shaker and WiFi-connected laptop 4
7. Geometry of the Olympus BTX-II benchtop XRD diffractometer 4
8. Vibrating sample holder (VSH) 5
9. Example of an XRD pattern (intensity, cps and 2θ, degrees) of a pure quartz sample 7
10. Example screenshot of Rietveld refinement of XRD data interpretation using Siroquant 9
11. Regional geology of the Greenbushes pegmatite deposit 13
12. Greenbushes Li deposit pegmatite specimen GSWA 201965 13
13. XRD pattern of the red mineral mixture in sample GSWA 201965 15
14. XRF spectrum of the red mineral mixture in sample GSWA 201965 15
15. XRD pattern (intensity, counts × 100 in cps and 2θ, degrees) of the red mineral mixture in sample GSWA 201965 16
16. Regional geology and location of the Corybas 1 well in the northern Perth Basin 17
17. Sandstone core chip analysed sample from 2506.13 m of Corybas 1 well 17
18. XRD pattern (intensity, cps and 2θ, degrees) of the Corybas 1 sample 18
19. XRF spectrum (intensity, cps and energy, keV) of the Corybas 1 sample 18
20. XRD pattern (intensity, cps and 2θ, degrees) of the Corybas 1 sample analysed using Siroquant 19

Tables

1. BTX-II measurement time recommended by Olympus 6
2. CSIRO laboratory semiquantitative XRD reporting thresholds 10
3. CSIRO powdered mineral and rock standards analysed by BTX-II 11
4. Comparison of calculated mineral compositions (weight %) using RIR analysis between the BTX-II and MRT laboratory XRD 11
5. Mineral composition of core samples from the Irwin River Coal Measures in Corybas 1 well analysed using BTX-II and AWE (2008) data 14
6. Mineral composition of core samples from the Irwin River Coal Measures in Corybas 1 well analysed using BTX-II and AWE (2008) data 19

Appendix

CSIRO powdered mineral and rock standards analysed by BTX-II 21

Appendix figures

A1. XRD pattern (intensity, cps and 2θ, degrees) of the powdered mineral standard BCS 368 21
A2. XRD pattern (intensity, cps and 2θ, degrees) of the powdered mineral standard KGa-2 21
A3. XRD pattern (intensity, cps and 2θ, degrees) of the powdered mineral standard SAz-1 22
A4. XRD pattern (intensity, cps and 2θ, degrees) of the powdered mineral standard H-33a 22
A5. XRD pattern (intensity, cps and 2θ, degrees) of the powdered mineral standard H-49 23
A6. XRD pattern (intensity, cps and 2θ, degrees) of the powdered rock standard G-2 23
A7. XRD pattern (intensity, cps and 2θ, degrees) of the powdered rock standard SY-2 24
A8. XRD pattern (intensity, cps and 2θ, degrees) of the powdered rock standard JB-1 24
A9. XRD pattern (intensity, cps and 2θ, degrees) of the powdered rock standard UM-2 25
A10. XRD pattern (intensity, cps and 2θ, degrees) of the powdered rock standard SARM 39 25

Application of rapid benchtop X-ray powder diffractometry for identification and characterization of mineral phases in geological materials

by

MJ Wawryk and EA Hancock

Abstract

The Olympus BTX-II benchtop X-ray diffractometer, recently acquired by the Geological Survey of Western Australia (GSWA), enables objective mineral identification and quantification of powdered geological samples by simultaneous collection of X-ray diffraction (XRD) and X-ray fluorescence (XRF) data. XRD data can be variously applied, including lithological classification and measurement of clay mineral crystallinity. The rudimentary coupled XRF elemental detection aids in phase identification, with detection limits observed to range from ~1% (e.g. As) to several hundred ppm (e.g. Sn).

Various geological samples were analysed using the BTX-II to test its capabilities and accuracy. Sandstone from the Irwin River Coal Measures of the Perth Basin, collected at 2506.13 m from drillcore of the Corybas 1 well, was calculated to consist of quartz (67.3%), microcline (14.5%), dickite (10.2%), muscovite (4.8%) and calcite (3.3%), consistent with reported petrology of nearby core samples using XRD and thin section microscopy. A red mineral phase in specimen GSWA 201965 from the Greenbushes pegmatite in the South West Terrane, visually identified as lepodolite (Li-bearing mica), was instead proven by XRD analysis to primarily consist of quartz and various zeolites. The identification of Cs in the XRF spectrum, but lack of a large pollucite 321 peak at ~3.66 Å, confirms the presence of a Cs-rich analcime member of the analcime–pollucite solid-solution series. The distinctive red colour of this phase is attributed to the presence of significant Mn detected by XRF.

KEYWORDS: mineral identification, petrology, Rietveld method, X-ray crystallography, X-ray diffraction, X-ray diffraction pattern, X-ray fluorescence, X-ray powder diffraction

Introduction

Mineralogical studies of rock and soil samples are fundamental to many of the projects undertaken by the Geological Survey of Western Australia (GSWA), which aim to improve the knowledge and understanding of the diverse natural resources and complicated geology of Western Australia (GSWA, 2016). Analysis of the physiochemical properties and distribution of minerals is routinely used in the discrimination and classification of lithological units, interpretation of formation conditions and origins, clarification of complicated metamorphic and alteration histories, and the identification and characterization of mineralizing systems (GSWA, 2016).

The value of this information is reflected by the continued investment in, and adoption of, new mineralogical analysis techniques by GSWA. Traditional petrographic studies of geological samples collected in the field or from drillcore are now complemented by data from new technologies, including elemental assays from portable X-ray fluorescence (XRF) spectrometers (Morris, 2009), high-magnification imagery from scanning electron microscopes, and hyperspectral drillcore linescans from the GSWA National Virtual Core Library (NVCL) HyLogger-3 (Hancock et al., 2013). The acquisition of a benchtop X-ray powder diffractometer (pXRD) adds to the analytical capabilities of GSWA, allowing rapid and inexpensive identification and characterization of minerals.

The pXRD was acquired by GSWA to enable independent validation of mineralogical identification and interpretations from hyperspectral logging or visual inspection of core and other geological materials. Improvements in technology and advances in computing power and software automation have significantly simplified data acquisition and subsequent analysis, permitting this technique to become a routine part of geological studies. The aim of this Record is to provide a brief introduction to benchtop X-ray powder diffractometry for novice users, instruct on the use and capabilities of this instrument, and present examples of how it can be used and integrated with other analytical techniques.

Fundamental principles of X-ray powder diffraction

X-ray powder diffraction (XRD) analysis is an established technique for the identification and characterization of minerals and other crystalline compounds. XRD of powdered samples relies on the assumption that crystal grains are randomly oriented in the powder, exposing equal and statistically significant numbers of all crystallographic planes for analysis (Sarrazin et al., 2005; Klein and Dutrow, 2007). Typically this requires samples to be crushed to a fine (<10 μm) powder (Bish et al., 1989);

however, this technique allows the analysis of mineral mixtures and fine-grained samples that are beyond the capabilities of single crystal X-ray diffractometers or optical microscopes (Sarrazin et al., 2005; Klein and Dutrow, 2007).

During XRD, crystalline samples are exposed to a beam of monochromatic (uniform wavelength) X-rays, which is scattered by the atoms forming the crystal lattices (Wilson, 1949; Klein and Dutrow, 2007). X-rays, which are electromagnetic waves of high energy and very short wavelength, are ideal for crystallographic analysis, with a wavelength comparable in magnitude to atomic spacings in crystal lattices, and high energies enabling penetration into crystal structures (Cullity, 1956; Klein and Dutrow, 2007). Crystallographic properties are derived from the angles and relative intensities of X-rays diffracted by crystal lattice planes during XRD, requiring all possible crystallographic orientations be observed for an accurate understanding of the analysed sample (Moore and Reynolds, 1989; Klein and Dutrow, 2007).

The Bragg theory of crystal diffraction describes crystals as parallel planes of atoms separated by distance 'd', and assumes that when a collimated beam of monochromatic X-rays (wavelength λ) strikes a crystal, each atom acts as an elastic scattering centre and emits a secondary wave (Wilson, 1949; Klein and Dutrow, 2007). The scattered X-rays destructively interfere and cancel out in most directions, but peaks in the intensity of scattered radiation will occur when X-rays from successive parallel planes of atoms interfere constructively, resulting in diffraction of the incident X-ray beam (Wilson, 1949; Klein and Dutrow, 2007).

The constructive interference due to the scattered waves being in phase with one another is described by Bragg's Law through the equation $n\lambda = 2d \sin\theta$ (Fig. 1). The geometry of Bragg diffraction can be considered simplistically as reflections from crystal lattice planes, but occurring only at specific angles that satisfy the conditions of the Bragg equation. However, not all possible Bragg diffraction angles will necessarily be detectable, due to systematic extinctions caused by the geometry of the fundamental crystal lattice unit cell (Cullity, 1956; Jenkins and Snyder, 1996). Diffracted X-ray beams are recorded on film or by an electronic detector, and their angle of diffraction to the incident beam (2θ) measured to derive the atomic spacing of the various crystal lattice planes (Moore and Reynolds, 1989; Klein and Dutrow, 2007).

In XRD of powdered samples, the random orientation of crystal grains to the incident beam results in the discrete X-ray diffraction spots from corresponding crystal planes creating a series of nested cones known as Debye–Scherrer cones (Fig. 2), each representing a specific angle of diffraction (Klein and Dutrow, 2007). These cones are intersected by 2D detectors as arcs of concentric rings (Debye–Scherrer rings), and counts of the X-rays used to measure the diffraction intensity of crystallographic planes (Moore and Reynolds, 1989; Klein and Dutrow, 2007). Poor particle statistics (insufficient number of crystal grains measured) result in incomplete or spotty Debye–Scherrer rings, causing random errors in observed diffraction peak intensities (Sarrazin et al., 2005). Similarly, preferential orientation of grains can result in crystallographic planes being favoured or disfavoured during diffraction, causing systematic errors in observed diffraction peak intensities (Brindley, 1961; Moore and Reynolds, 1989).

Powder diffraction patterns

The results of XRD analyses of powdered samples are typically presented as diffraction patterns (diffractograms) of narrow peaks with varying heights and half-widths, representing measured counts of diffracted X-rays recorded by the detector arranged by the angle of their detection (Fig. 3). As the atomic spacing in any given crystallographic plane increases, the resulting diffraction peaks will occur at lower angles as defined by Bragg's Law. The relative intensity of diffraction peaks (the total area of a peak, which is typically equivalent to its height) varies due to many complicated factors not detailed in this Record, such as the average atomic mass of an atomic plane, the number of equivalent scattering planes in a crystal, absorptions and polarization (Cullity, 1956; Moore and Reynolds, 1989; Klein and Dutrow, 2007).

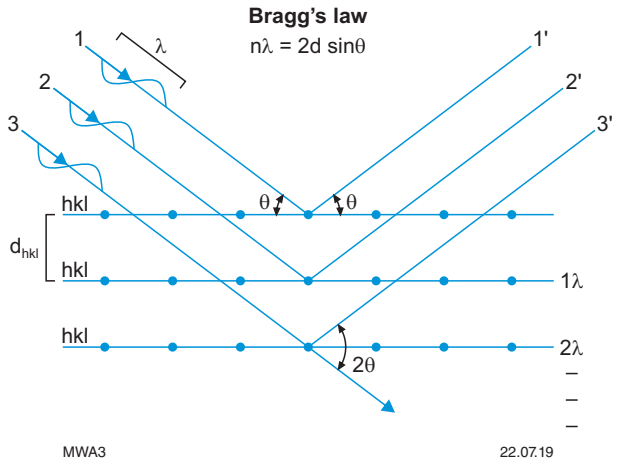

Figure 1. **Bragg's diffraction diagram showing monochromatic X-rays of given wavelength (λ), width of the spacing (d_{hkl}) between planes of atoms of lattice plane hkl, X-ray incidence angle (θ), and diffraction angle (2θ). From Veqter Ltd (2019)**

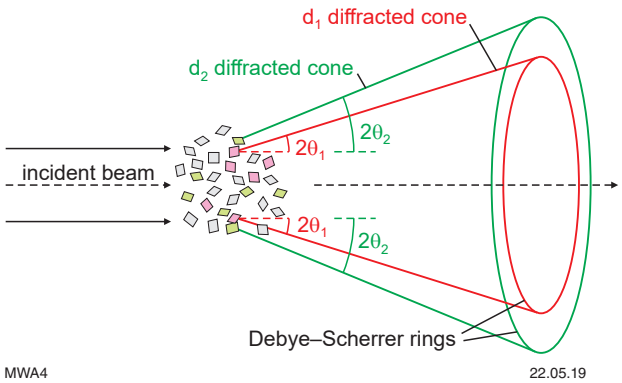

Figure 2. **Diagram of Debye–Scherrer diffraction cones d_1 and d_2; $2\theta_1$ and $2\theta_2$ are diffraction angles of incident beam from random oriented crystallites with atomic plane spacings d_1 and d_2. From Barnes et al. (2016)**

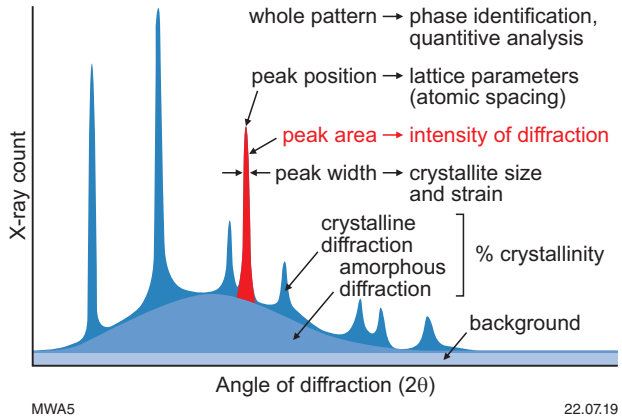

Figure 3. Diagram of an X-ray diffraction pattern, displaying measured counts of X-rays by the measured angle of diffraction (2θ), and the various crystallographic parameters that can be determined from the pattern. The overall pattern is a composite of background radiation, and diffraction by crystalline and amorphous phases. Modified from Alagarsamy (2016)

Variations in the crystallographic arrangement, atomic spacing and elemental composition between different crystalline phases result in unique idealized XRD patterns, allowing qualitative identification even between solid-solution end-members or mineral polymorphs (Klein and Dutrow, 2007). The identification of materials by XRD analysis is based upon matching the relative intensities and locations of peaks in an XRD pattern, to those from known compounds, often referred to as 'fingerprinting' (Moore and Reynolds, 1989; Klein and Dutrow, 2007). The complexity of this task is dependent on the number of unique phases present in a sample, as XRD patterns for mixed samples are a composite of the XRD patterns of the individual phases, and overlapping of peaks can occur (Brindley, 1961; Moore and Reynolds, 1989). Further complexity is added by deformation of the crystal structures and the degree of crystal ordering (Cullity, 1956; Jenkins and Snyder, 1996).

Uniform strain (macro-strain) of a crystal lattice causes slight changes to the unit cell parameters, resulting in the positions of diffraction peaks shifting (Cullity, 1956). Similarly, non-uniform strain (micro-strain) of crystallites, including by vacancies and dislocations, results in the broadening of diffraction peaks (Cullity, 1956; Moore and Reynolds, 1989). Poorly ordered or amorphous material will not cause diffraction only at characteristic angles, due to the lack of long range atomic ordering preventing perfect destructive interference at non-Bragg angles, instead creating broad peaks that elevate the intensity of the background in the XRD pattern (Fig. 3; Cullity, 1956). These effects can be useful, however, as the identification and quantification of crystallinity and crystal lattice alteration can be useful for metamorphic studies (Doublier et al., 2010). Peak broadening is also observed with reduction in crystallite size, although this effect is only significant for crystallites below 0.1 µm (Cullity, 1956; Jenkins and Snyder, 1996).

X-ray fluorescence

If sufficiently excited by incident X-radiation, such as during XRD, electrons in the inner shells of the target atoms can be dislodged and are replaced by higher energy electrons from the outer shells (Fig. 4; Klein and Dutrow, 2007). In filling the inner shell vacancies, outer shell electrons lose excess energy by emission of secondary X-rays with specific wavelengths (energy), a phenomenon referred to as X-ray fluorescence (XRF) (Klein and Dutrow, 2007; Morris, 2009). The wavelengths of secondary X-rays produced during XRF correspond to the difference in energy between the electronic states of the transition, and are characteristic of their atomic element (Klein and Dutrow, 2007). The elemental composition of samples can thus be determined by measuring the energy or wavelength of X-rays produced by XRF, and their relative abundance (Fig. 5; Morris, 2009).

Consideration of XRF must be made during XRD analysis, as it can impact the quality and appearance of XRD patterns. In contrast to diffracted incident X-rays which are scattered at specific and discrete angles, the emission of secondary X-rays by XRF occurs at random angles and varying wavelengths, resulting in the increase of the background (Fig. 3) in XRD patterns (Cullity, 1956; Jenkins and Snyder, 1996). The absorption of incident X-radiation during XRF simultaneously reduces the amount of incident X-radiation that is diffracted, weakening the intensity of diffraction peaks and reducing the overall peak-to-noise ratio (Cullity, 1956; Mitra, 1996). These issues are partly addressed by filtering out or blocking X-rays of different wavelengths to the incident X-ray beam (Cullity, 1956), and selection of a suitable X-ray sources to minimize fluorescence from the sample (Brindley, 1961; Mitra, 1996).

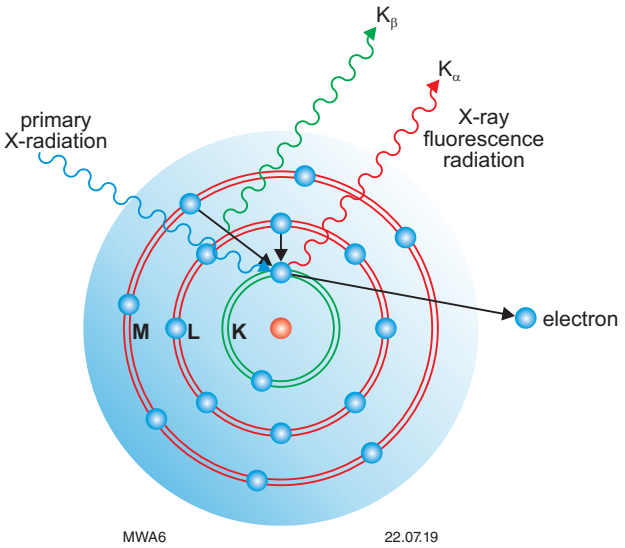

Figure 4. Diagram of X-ray fluorescence, showing incident X-ray causing the ejection of an excited inner-shell electron, and resulting emission of secondary X-rays from the replacing outer-shell electron. From Fischer Instrumentation (GB) Ltd

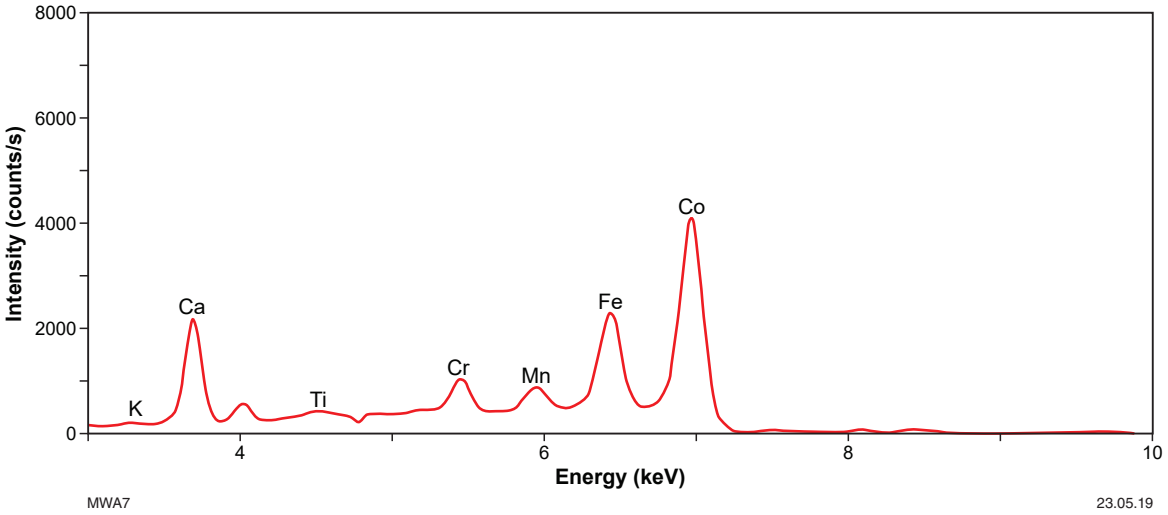

Figure 5. **Example of an X-ray fluorescence pattern, displaying intensity in counts per second (cps) by the measured energy of the X-rays (keV). Peaks are labelled according to the originating atomic element, by matching the energy of peaks to known characteristic energies. Modified from Olympus (2014, fig. 4–7)**

The benchtop X-ray diffractometer

In 2014, GSWA purchased an Olympus BTX-II benchtop X-ray diffractometer (Fig. 6) for analysis of powdered geological samples, to complement work carried out at GSWA's Perth Core Library and HyLogger-3 facilities. Derived from and employing the same pioneering technology developed by NASA for the 2011 Mars 'Curiosity' rover mission, the BTX-II is a portable system for XRD analysis and coupled rudimentary XRF analysis with minimal sample preparation requirements (Bish et al., 2014). Although fully portable, the BTX-II is intended for benchtop work in contrast to the rugged Terra field portable equivalent.

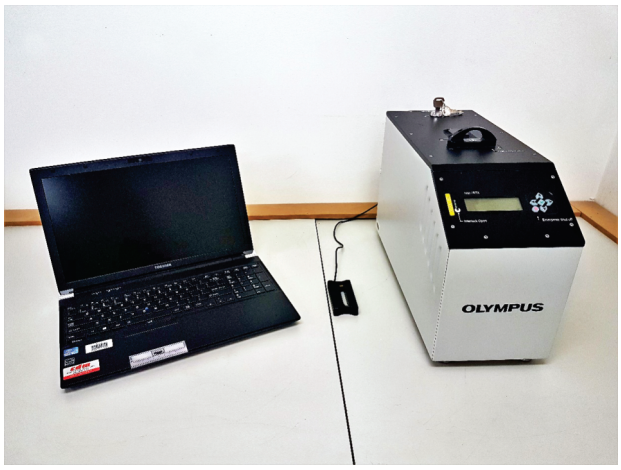

Figure 6. **The GSWA benchtop XRD with external shaker and WiFi-connected laptop**

Instrument hardware

The BTX-II consists of three basic elements: a collimated micro-focus X-ray source, a vibrating transmission sample cell, and an X-ray sensitive charge-coupled device (CCD, Fig. 7; Olympus, 2014). The fixed transmission geometry and lack of moving components in the BTX-II reduces its size (0.3 × 0.17 × 0.47 m), weight (12.5 kg) and complexity compared to conventional laboratory-based instruments. A cobalt-anode ($K\alpha^{-}$=1.7902 Å) was chosen for the X-ray source (30 kV, 10 W), as it enables analysis of a greater range of atomic spacings for the given 2θ detection range than the standard Cu-anode, and measurement of the large atomic spacings critical for analysis of clay minerals. In addition, Fe strongly fluoresces when using a Cu-anode, compared to Ca and Mn when using a Co-anode, which was of particular concern due to the prevalence of Fe-rich rocks in Western Australia.

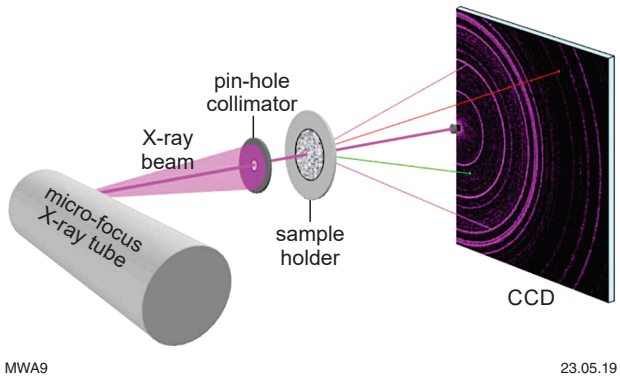

Figure 7. **Geometry of the Olympus BTX-II benchtop XRD diffractometer. Reproduced from Blake et al. (2009, fig. 2)**

A 50 µm collimated X-ray beam is transmitted through the sample cell (see discussion below), and the resulting X-rays detected by an energy-discriminating CCD (Olympus, 2014). The ability of the CCD detector to measure both the position and energy of transmitted X-rays allows the discrimination of X-rays generated by XRF from diffracted X-rays, and hence the simultaneous generation of 2D XRD patterns and XRF histograms for analysis. The embedded InXitu software controls operation of the BTX-II and access to the generated X-ray data stored on an internal hard drive, and is accessed through the web browser of a computer linked by Ethernet cable or via the in-built wireless network connection (Olympus, 2014).

Vibrating sample holder

The BTX-II uses a spring-loaded piezo-harmonic vibrating sample holder (VSH) to agitate and circulate sample grains during analysis (Fig. 8; Olympus, 2014). The resulting motion of the sample exposes more crystallites to the incident X-ray beam, which greatly improves particle statistics of the analysis (Sarrazin et al., 2005). The vibration also randomizes grain orientations, virtually eliminating the preferential orientation effects of specific minerals (e.g. micas, chlorites), which impact other XRD instruments (Sarrazin et al., 2005) and cause overestimation of their abundance (Uvarova et al., 2014; Burkett et al., 2015). The resulting improvement in the XRD pattern enables the analysis of coarser samples (<150 µm vs <10 µm) and smaller sample amounts (~20 mg vs 200–300 mg) compared with traditional laboratory-based XRD instruments (Sarrazin et al., 2005).

Powdered samples are loaded into a sample cell for analysis, which is attached to the VSH by screws (Fig. 8). Sample loading is assisted by an external sample shaker, which replicates the vibrations applied to the VSH during analysis. The sample cells consist of two X-ray transparent thin polymer film windows (Kapton or Mylar), with a thin aluminium spacer (currently 175 µm wide) between cells to hold the sample. Kapton windows are preferred for their robustness; however, their use results in a significant 'Kapton peak' appearing in XRD patterns at ~6.7° 2θ, which can mask phyllosilicate 001 peaks (Bish et al., 2014). If an important peak in this region is expected from the sample (e.g. presence of phyllosilicates), the more fragile Mylar windows should be used, which create a broad 'Mylar peak' at ~19° 2θ instead (Bish et al., 2014).

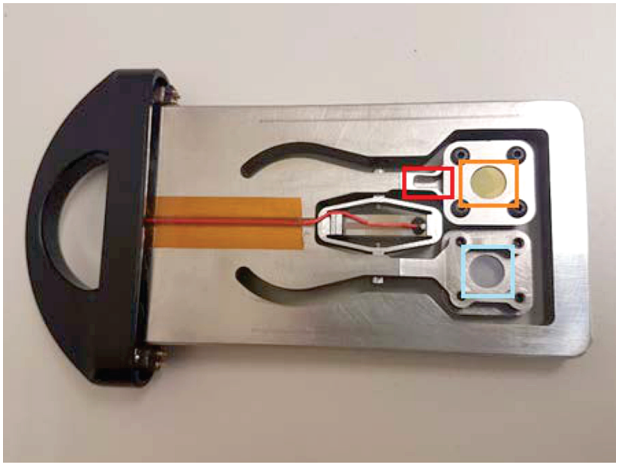

Figure 8. Vibrating sample holder (VSH) with sample feeding chutes (red box) and attached sample cells. Sample cells consist of two X-ray transparent thin polymer windows of Kapton (orange box) or Mylar (blue box), and a thin aluminium spacer between to hold the sample

Significant density differences of particles in the mixture may lead to enhanced vertical segregation during sample vibration, resulting in overestimation of heavy minerals and underestimation of light minerals by several percent by volume (Bish et al., 2014; Burkett et al., 2015). The effect of this phenomenon on quantitative analysis is particularly important due to the small volume of samples being analysed. At present, this density segregation is reported for artificial mixtures of single mineral phase particles, whereas natural mixtures of multiphase powdered rocks are not reported to show a pronounced segregation effect (Bish et al., 2014; Burkett et al., 2015).

Detection limits

The BTX-II has a 5–55° 2θ range, with a resolution of 0.25° full width at half maximum (FWHM; Olympus, 2014). This allows measurement of atomic spacing between 1.94 and 20.52 Å with the Co-anode, sufficient for analysis of most mineral phases. The compact transmission geometry of the instrument permits the detector to be positioned close to the sample, enabling the measurement of X-ray diffraction signals with equivalent intensity to higher powered laboratory-based XRD instruments. Similarly, the use of a 2D detector enables the simultaneous measurement of the entire 2θ detection range, and X-ray collection from greater portions of the Debye–Scherrer diffraction rings. This improves counting statistics compared to linear scan-based instruments, reduces errors due to poor particle statistics, and enables short analytical times comparable to high performance detectors.

The BTX-II has a detection limit of ~1% by volume for most minerals, 0.25% for quartz, and ~2–4% for clays. The greatest analytical limitation results from the relatively large FWHM compared to laboratory-based XRD instruments, which impedes the resolution of closely occurring diffraction peaks (Bish et al., 2014). This complicates the identification and differentiation of phyllosilicates and particularly clay minerals, as the large atomic distances of their crystal lattices create diffraction peaks at low angles, where the XRD pattern is most compressed and hence peak attribution is most difficult to determine (Bish et al., 2014). The complexity and variation in crystal structure of clay minerals means that laboratory XRD determination typically requires extensive sample preparation, including clay separations and various treatment techniques (Moore and Reynolds, 1989). Similar techniques might be employed for the BTX-II, although the instrument is better suited as a screening tool to rapidly identify the presence of these clay minerals in mixed composition samples.

The BTX-II also has a corresponding XRF detection range of 0–25 keV (3–15 keV typically used), with a maximum resolution of 250 eV at 5.9 keV (Olympus, 2014). The XRF detection capability of the BTX-II is rudimentary compared

to dedicated handheld XRF analysers routinely used by GSWA (Morris, 2009) and cannot provide full elemental analysis. Qualitative elemental analyses are performed using the positions of broad peaks in the XRF spectra, which correspond to characteristic energies of the various elements, and can be used to detect all naturally occurring elements between K and U. Instrument-originated Co, W, Cr, Mn and Fe are present as background signatures in the XRF spectra, and must be accounted for during analysis for an accurate understanding of elemental compositions. Significant elevation in peak intensity of these elements in the XRF spectra of a single analysis — compared to analysis of a pure quartz standard — can be used to infer their physical presence in a sample.

The lower limit of detection for the various elements are not yet sufficiently quantified and would vary between samples due to sample-dependent factors discussed in detail by Morris (2009), but in practice would typically range from several hundred ppm (e.g. Sn) to ~1% (e.g. As), based upon comparison with handheld XRF data. The coupled XRF capability of the BTX-II assists the XRD analysis, allowing filtering of potential diffraction peak matches by chemistry, and aiding with discrimination between end-members of mineral solid solutions (e.g. feldspars, chlorites, carbonates).

Sample preparation and operation

The design of the BTX-II allows for analysis of samples with minimal preparation; detailed preparation instructions with visual aids are available in Olympus (2014). To prepare a powder for analysis, samples are placed in the supplied sample crusher and broken down to a powder by repeated impact with a hammer, then dry-sieved to <150 μm using the sample sieve. The VSH is then inserted into the external shaker, and a micro-spatula used to feed ~20 mg of the sieved powder into the sample cell via the feeding chute above (Fig. 8). Ideally the sample cell should be two-thirds filled so that the sample can circulate, which can be visually assessed with the aid of the external shaker.

The small amount of samples required by the VSH provides the flexibility of analysing bulk samples or individual minerals, and samples can be recovered for future analysis. Single mineral grains and even wet samples can be analysed using the BTX-II, with consequently longer acquisition times and lower resolution results. The VSH is also equipped to hold a second sample cell, allowing preparation of multiple samples at once, although only one sample can be analysed at a time. Once the sample has been fully prepared, the VSH is inserted into the main instrument for analysis.

The BTX-II is fully contained, and a safety interlock is used to prevent operation if the VSH is inserted incorrectly, so no safety precautions are required by the operator (Olympus, 2014). Analysis of the sample is controlled using the InXitu software, which provides continuous visual updates of the X-ray data for monitoring purposes. X-ray data analysis is undertaken by the instrument in 10-second measurement windows (integration time) at a rate of 4.5 measurements per minute, with the sample circulating continuously throughout. Analysis should be continued until sharp diffraction peaks and high peak-to-background ratio are obtained, with manufacturer-recommended analytical times ranging from 5 to 45 minutes (Table 1). However, recent studies by Uvarova et al. (2014) and Burkett et al. (2015) have demonstrated that analytical run-times of 5–10 minutes with equivalent instruments is sufficient for accurate quantitative results comparable with laboratory-based XRD analysis, although the accuracy for minor phases was noted to improve with longer analysis times.

Table 1. BTX-II measurement time recommended by Olympus

Analytical purpose	*Analysis time*
Single phase identification	2–5 minutes
Major phase identification	5 minutes
Minor phase identification	10–20 minutes
Compositional quantification	10–20 minutes
Clay identification	30–45 minutes

A powdered quartz standard is run at the beginning of every analytical session, and after every tenth analysis, which aids in cleaning of the polymer windows. The quartz standard is used to calibrate the data and detect peak drift, with diffraction peaks from quartz expected to coincide with reference lines in the InXitu interface (Fig. 9). Other mineral standards can also be used for this purpose, although quartz and beryl are particularly well suited due to their low absorption coefficients for cobalt X-radiation, and the presence of multiple intense peaks in the 5–55° 2θ range (Bish et al., 2014). Between analyses, the sample cell windows should be gently cleaned with ethanol or compressed air to prevent cross contamination, and preparation equipment should also be cleaned between samples.

Data and analysis

Data generated by the BTX-II is stored on an internal hard drive, and saved in a variety of formats that makes it compatible with a wide range of other analytical software (Olympus, 2014). Individual datasets are generated for each separate analysis, which can be accessed and downloaded through the InXitu interface on a connected computer. Datasets (typically 2–10 MB each) include automatically generated plots (.png, .eps), tables of X-ray data (.txt, .uxd, .ruf), and images of the X-ray detection patterns equivalent to traditional film exposures (.tif). XRF data is contained in separate files from XRD data.

XRD data from the BTX-II are divided into unfiltered 'film' files that utilize all detected X-rays, and filtered 'ka' files that only utilize X-rays with the same measured energy as the source X-rays. Film files (e.g. Name-film.txt) are preferred for analysis unless significant fluorescence is detected (i.e. elevated background in diffraction pattern), as the higher X-ray detection counts and consequently improved signal-to-noise ratio makes peak identification easier. The presence of amorphous phases will create broad areas of elevated background in the XRD patterns

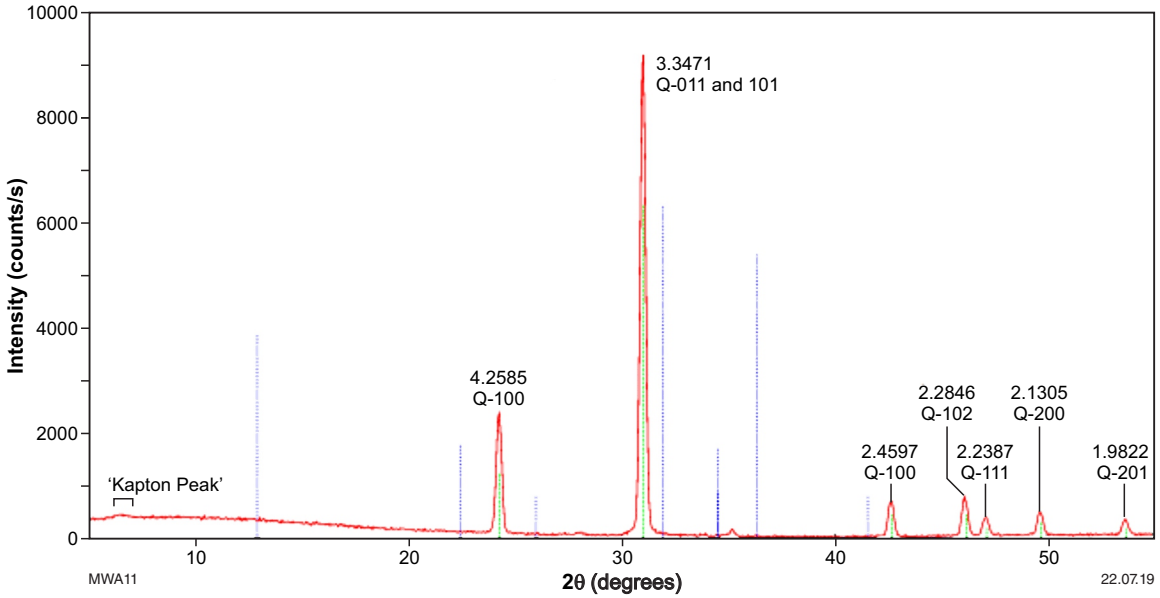

Figure 9. Example of an XRD pattern (intensity, cps and 2θ, degrees) of a pure quartz sample from the GSWA pXRD. Observed peaks have been labelled by their corresponding atomic spacing and attributable crystallographic planes. Note the small Kapton peak" at ~6.5° 2θ, and the green and blue reference lines used to visually calibrate the data, which represent the expected peaks for quartz and beryl respectively

similar to those created by XRF (Cullity, 1956), but in contrast these elevated backgrounds will not be removed by energy-based filtering (e.g. use of 'ka' files), as the energy of incident X-rays are not altered during diffraction. Most analytical XRD software allows quick visual background removal, making the assessment of relative peak intensities and peak identification easier.

Qualitative analysis

Mineral phase identification

Qualitative phase identification of materials analysed by XRD is performed by 'fingerprinting', the process of systematically matching the relative intensities and locations of peaks in an XRD pattern to those from known compounds, until all measured diffraction peaks are attributed to a phase (Moore and Reynolds, 1989; Klein and Dutrow, 2007). Various analytical software and XRD phase pattern databases are available to assist in this task, including the commercial XPowder software package (www.xpowder.com) purchased by GSWA for staff to analyse data generated by pXRD. Although preference here is given to description of XRD analysis using the XPowder software, the general methods are described broadly and can be universally applied. Detailed instructions for the use of the XPowder software package are provided in the XPowder user guide (Martin, 2012).

XPowder enables qualitative crystalline phase identification through peak matching using the incorporated American Mineralogist Crystal Structure Database (AMCSD; www.minsocam.org/MSA/Crystal_Database), which includes 80 000 XRD reference patterns for over 5000 minerals. New reference patterns can be created in XPowder for mineral phases not included in the AMCSD, and reference data can be imported from other XRD databases, such as the International Centre for Diffraction Data (ICDD; www.icdd.com) databases and RRUFF project (www.rruff.info). The mineralogical database Webmineral also provides a free searchable database of the most intense XRD peaks of over 6400 mineral samples (http://webmineral.com/help/XRayDiffraction.shtml#.WqYhA-S7qUl).

A general workflow for mineral phase identification involves loading both ka.txt and film.txt files (energy-filtered and unfiltered plain text tables of X-ray counts by 2θ angle of detection) into XPowder, and visually comparing the respective patterns using the stack screen. If all the peaks in the unfiltered film.txt pattern are present in the filtered ka.txt pattern, and there is no observable fluorescence, then the film.txt pattern should be used for analysis due to the previously discussed signal-to-noise ratio improvement. Removal of the background should then be applied to the XRD pattern using the in-built 'Background Subtraction' feature, and the pattern algorithmically smoothed using the 'Fourier Smoothing' tool, which both aid the user to identify diffraction peaks and correctly estimate their intensity. Finally, the user identifies and measures diffraction peaks either by manual selection, or with the aid of an automated peak searching tool such as the 'Bragg Peak Search' feature.

Users can search the in-built database to find phases to match peaks in the diffraction pattern, systematically identifying the causative phase of the most intense unexplained peak in the pattern, and continuing until all observed diffraction peaks are attributed to a mineral phase. Reference patterns are displayed as vertical lines representing expected peak locations and intensities, enabling visual elimination of unsuitable matches indicated by peaks in a reference pattern being absent from the recorded pattern. Knowledge about likely mineral phases

based upon geological context, known chemistry of the sample, or observation of characteristic diffraction peaks (e.g. strong quartz peak at 3.34Å) is useful in refining possible matches for the measured diffraction pattern. Possible phase matches can be automatically identified from the positions of one or multiple selected peaks using the 'One click searching' tool in XPowder, or manually found by searching the pattern database by elemental chemistry or phase name.

Positions of diffraction peaks should be reported by their corresponding atomic spacing, as the 2θ angle will vary with the wavelength of the X-ray source. Difficulties will arise when attempting to match observed diffraction peak positions by 2θ angle to measurements made using a different X-ray source (e.g. Cu-anode), unless appropriate conversion calculations are made. As a result, many modern XRD pattern databases such as the AMCSD and Webmineral database report diffraction peak locations by their corresponding atomic spacing instead, or provide conversion tools for common X-ray anode sources.

Elemental identification

Analysis of XRF spectra is complementary to XRD phase analysis described above, providing information about the elemental composition of phases in the sample. Elements detected in the associated XRF spectrum can be used to refine possible phase matches in measured diffraction patterns, including discriminating between end-members of solid-state solutions (e.g. carbonates and feldspars). The InXitu interface generates a simplified plot of the measured XRF spectrum (Fig. 5), and automatically identifies the corresponding elements of the most prominent fluorescence peaks. However, significantly more elements can be identified by measurement of smaller peaks in the XRF spectra, which are not automatically detected by the InXitu software.

XRF data measured by the BTX-II is recorded in 'Name-xrf.txt' files as a plain text tables of measured X-ray counts by measured X-ray energy. Although no specialized XRF analysis software has been obtained by GSWA, simple analysis can be made by plotting the measured data in MS Excel or similar software, and comparing the positions of peaks (keV) to known characteristic X-ray energies. The measured characteristic transition energies of the various elements are widely available from numerous sources, including the X-ray Transition Energies Database (https://physics.nist.gov/PhysRefData/XrayTrans/Html/search.html).

Quantitative analysis

Reference intensity ratio analysis

XPowder allows quantitative estimation of different phases in a sample, using the Reference Intensity Ratio (RIR) method. The RIR method is based upon scaling all diffraction data relative to the diffraction of standard reference materials, with the intensities of diffraction peaks known to be related to the abundance of a phase in a mixture (Chipera and Bish, 2013). By convention, corundum is used as the international reference phase, and the scaling factor is defined by Intensity of an Analyte / Intensity of Corundum (either for the most intense peak or full pattern) in a 50:50 mixture of the analyte with the corundum standard (Chipera and Bish, 2013). The RIR method allows direct comparison of various phases in the powdered sample, and the relative abundance of the phases to be obtained from their measured intensity in the mixture (Chung, 1974). This method is simple and provides relatively accurate estimation of the mineral composition without user expertise (Chung, 1974; Chipera and Bish, 2013).

XPowder stores the RIR values for most of the minerals in its database, enabling RIR analysis of identified phases in the measured XRD pattern. Users are also able to spike measured samples with a known amount of an internal standard, which allows for the quantification of amorphous phases (Chung, 1974; Chipera and Bish, 2013). However, the RIR method is sensitive to factors such as variable chemistry and preferred orientation of phases, which alter the location and relative intensities of diffraction peaks compared to standard profiles (Chipera and Bish, 2013). Because of the difficulties in estimating amorphous content without an internal standard, and the distortion of calculated compositions caused by variations in measured diffraction peaks of a phase to reference patterns, the results of RIR analysis in XPowder are treated as semiquantitative.

Rietveld refinement

Alternatively, quantitative phase compositions can be calculated from diffraction patterns using the more complex and powerful Rietveld refinement method. The Rietveld refinement method uses least squares regression analysis to refine a modelled theoretical diffraction pattern until it matches the measured pattern, allowing modelled phases and their crystallographic properties to be adjusted to accurately fit the measured profile, and the relative proportion of phases to be calculated. In addition to phase quantification, Rietveld refinement allows determination of other crystallographic factors including crystallite size and strain, unit cell parameters and atomic occupancies (Bish and Howard, 1988; Chipera and Bish, 2013).

Although various analytical software can be used to perform Rietveld refinement of XRD data, preference is given here for description of the method using the Siroquant software package (www.siroquant.com), which was also purchased by GSWA for advanced analysis of data generated by pXRD. Detailed instructions for the use of the Siroquant software package is provided in the Siroquant User Manual (Sientronics Pty Ltd, 2007) and Technical and Clays Manual (Sientronics Pty Ltd, 2006). Siroquant is not suited for qualitative identification of mineral phases in a sample, due to its limited mineral phase library and lack of peak matching functionality. Phases present in the analysed sample should be determined first by peak matching (e.g. using XPowder), before the data is analysed in Siroquant.

Users are able to import XRD patterns measured by the BTX-II directly into Siroquant using the generated .txt files. Once the desired phases for modelling are selected and background subtraction is performed, a preliminary refinement is performed to scale the patterns of the corresponding phases to the measured XRD pattern. The resulting model is automatically displayed across the

measured pattern. Siroquant will also generate a differential plot of the variance between the measured and modelled patterns (Fig. 10), along with a mathematical measure of fit of the whole modelled pattern (R-factor, perfect fit is 0) and a measurement of model refinement (χ^2 or chi-squared, perfect fit is 1). The model should be systematically refined (crystallographic parameters adjusted) until the differential pattern or χ^2 value is minimized, which will correspond with the best fitting model. Although a perfect model fit will result in a χ^2 value of 1, Hillier (2000) found in practice that a model of good fit will generally have a χ^2 value between 3 and 5.

The shape and size of the greatest deviations in the differential pattern, which directly correspond to the areas of poorest fit, are used to visually identify the phases and corresponding parameters to adjust. Siroquant provides a simple user interface, allowing the user to nominate which parameters to adjust, which is then performed iteratively by the software. Mismatches in modelled and actual peak locations are initially rectified globally by adjusting the instrument zero, and then peaks of individual phases can be adjusted using the crystal dimension parameters (a, b, c etc.). Poor fit of peak widths are adjusted using the linear half-width parameter (W), to account for issues such as micro-strain or crystal defects. Poor fit of peak heights is similarly adjusted using the preferred orientation parameter. At each stage, adjustment to the scale of the phases should be made, as this will affect the calculated weight of the phases.

Advanced users are also able to adjust various other parameters in Siroquant such as extinctions, absorptions and temperature effects, although these parameters can generally be ignored for most simple operations. The relative proportions of the phases in the model are recalculated by Siroquant throughout the refining process, but should only be reported once the model has been optimized. Other factors such as crystal dimension parameters, proportion of amorphous phases, and crystallite size can also be calculated by Siroquant once the model is optimized, providing further crystallographic and geologic information from the measured XRD pattern. The merit of refinement parameters is displayed by Siroquant after each refinement calculation, using a plot of calculated χ^2 at each stage of the refinement for the whole pattern and individual phases. A downwards trend in χ^2 (towards 0) reveals improvement in the model during refinement, with an upwards trend conversely indicating that a refinement factor is reducing the fit of the model.

Rietveld refinement is known to provide accurate measurement of mineral compositions, but requires significantly more user experience and knowledge than the RIR method used in XPowder (Ward and Gómez-Fernández, 2003; Uvarova et al., 2014; Burkett et al., 2015). As such, RIR analysis is recommended for less-experienced operators. When reporting the results of quantitative X-ray analysis using XPowder, however, relative terms should be used when referring to mineral abundances, due to the previously mentioned difficulties and issues with quantifying amorphous content. Examples of the relative thresholds used by the Commonwealth Scientific and Industrial Research Organisation (CSIRO), and subsequently adopted for reporting the results of GSWA pXRD analyses, are listed in Table 2.

Clay mineral identification

Identification of clay minerals by XRD analysis is known to be inherently complicated, due to the structural similarities shared by these minerals, and their proclivity for chemical and physical variation (Brindley, 1961; Moore and Reynolds, 1989). As a result of shared structural elements, related clay minerals species commonly create

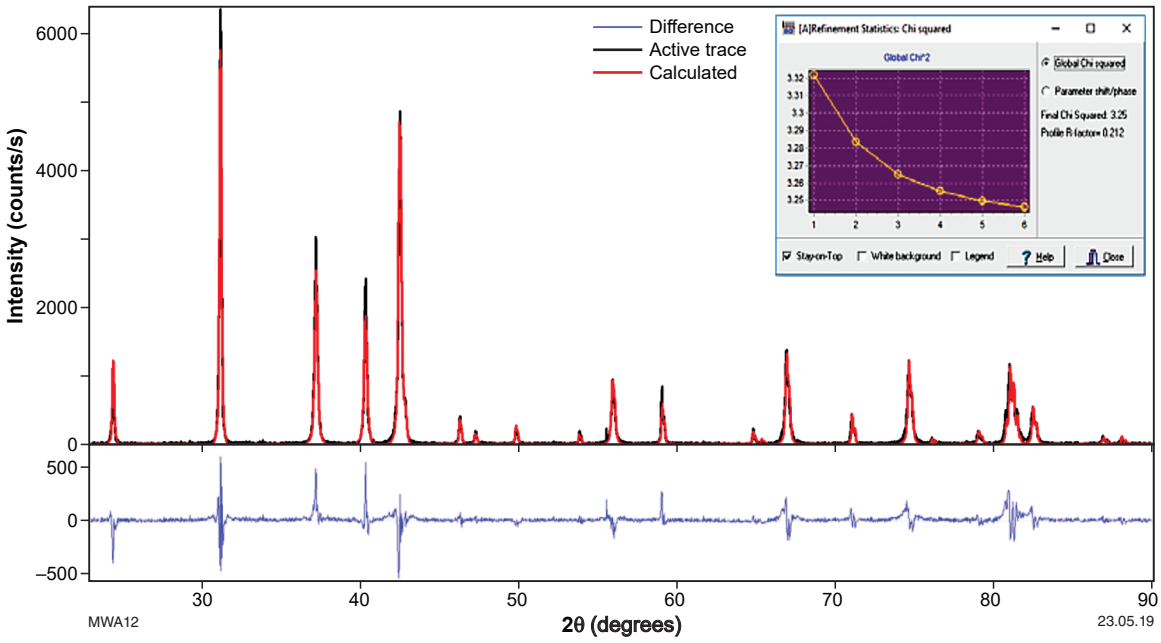

Figure 10. Example screenshot of Rietveld refinement of XRD data interpretation using Siroquant software, showing measured XRD pattern (black), generated model (red) and differential plot (blue), and displayed as intensity (cps) by 2θ angle of diffraction (degrees). The inset window provides a mathematical measure of fit of the model (χ2), and provides a visual representation of its change during stages of refinement. The analysed XRD pattern represents a 50:50 mixture of quartz and zinc oxide as measured by a laboratory-based XRD

Table 2. CSIRO laboratory semiquantitative XRD reporting thresholds

Title	*Proportion (by volume)*
Dominant	>50%
Major	20–50%
Minor	10–20%
Accessory	2–10%
Trace	<2%

similar diffraction patterns, with significant diffraction peaks often occurring at near or identical angular positions (Brindley, 1961; Moore and Reynolds, 1989). Even distinct clay mineral groups are known to cause issues with peak overlap, such as the overlap of even-order chlorite 00l peaks with kaolin 00l peaks (Moore and Reynolds, 1989). The issue of peak overlap is particularly problematic in mixed clay mineral samples, as the discrimination of separate species in such cases can be difficult, and misidentification can significantly impact the calculation of mineral proportions.

Although slight differences in diffraction peak locations can be used to discriminate between clay minerals, the relatively low angular resolution of the BTX-II can make this task difficult. Instead, the presence or absence of distinguishing diffraction peaks is preferred for qualitative identification. Mixed layer clay minerals are often identified using distinguishing diffraction peaks corresponding to large atomic spacings, which occur at very low angles (Moore and Reynolds, 1989). The inability of the BTX-II to measure diffraction peaks below 5° 2θ makes this instrument inherently unsuitable for analysing such crystal structures, without altering the X-ray source.

Further difficulties arise from variations in chemistry and crystallinity of clay minerals. Structural changes caused by cation exchange in clay minerals is known to shift the position and relative intensities of diffraction peaks, resulting in deviations from standard diffraction patterns (Brindley, 1961; Moore and Reynolds, 1989). Differences in crystallinity cause similar deviations from standard patterns, notably causing diffraction peaks to broaden and become more indistinct with increased disordering (Moore and Reynolds, 1989).

Measurement of this phenomenon in various phyllosilicate minerals is useful, however, in characterizing metamorphic or diagenetic grades of samples. Illite crystallinity (Kübler index: FWHM of ~10Å 001 peak) and chlorite crystallinity (Árkai index: FWHM of ~7Å 002 peak) are known to increase (smaller FWHM) with metamorphic grade (Árkai, 1991; Doublier et al., 2010). Though yet to be tested, measurement of these crystallinity indexes for samples from low-grade metamorphic and diagenetic environments should be possible with the BTX-II, although the FWHM resolution limit of 0.25° 2θ would inhibit measurement of crystallinity in samples beyond the anchizone (Árkai, 1991).

Well-established clay separation and treatment techniques such as inducing swelling with glycerol or ethylene glycol, and heating samples to various temperatures to induce structural decomposition (Brindley, 1961; Moore and Reynolds, 1989), traditionally address the problem of identifying clay minerals by XRD analysis (Moore and Reynolds, 1989). These techniques are used to enable the separation of individual clay mineral phases for further analysis, and to induce diagnostic structural changes. XRD analysis of clay minerals can also be supplemented by other analytical methods, including infrared spectroscopy and scanning electron microscopy (Brindley, 1961; Moore and Reynolds, 1989).

Clay separation and treatment techniques are time consuming, can be destructive, and require the user to have adequate expertise and training. However, the main purpose of the BTX-II is to provide rapid mineralogical and crystallographic analysis of geological samples without significant preparation requirements or user expertise. Therefore, the BTX-II is better suited for rapid analysis and screening of samples, and more sensitive X-ray diffraction techniques and instruments can be used subsequently if desired.

CSIRO powdered standards

The quality control of the GSWA pXRD performance was initially conducted on powdered international mineral and rock standards provided by CSIRO (Table 3). The purpose of the test was to confirm if the BTX-II repeatedly produced patterns associated with standard mineralogy, and its applicability to the wide range of GSWA samples. The powdered samples were also analysed using various analytical times (5, 10, 20, 30 and 40 minutes), to observe the effects of increased integration (time used by the sensor to collect X-ray photons). Diffraction patterns generated using the powdered mineral samples were found to be consistent with standard patterns of these minerals (Appendix Figs A1–10).

XRD analysis of the powdered standards using the BTX-II produced consistent diffraction patterns in each case, with distinct diffraction peaks suitable for qualitative identification observable within 5 minutes. Minor improvements in peak-to-noise ratio were noted with increased analytical times, which made peak identification easier particularly for minor phases. The distinct differences in observed diffraction patterns of rock standards indicate that representative patterns of measured sample lithologies could be used to rapidly characterize unknown samples without identifying specific mineral species.

Observed divergence in the position and relative intensities of some diffraction peaks for the powdered clay standards likely reflect chemistry differences between the powdered standards and the AMCSD standards due to cation exchange. Similar divergence can be expected in local clay minerals, due to differences in source geochemistry and geological histories. A case may be made to build a new (additional) reference library of diffraction patterns of local mineral and rock samples, to improve qualitative and quantitative analysis.

Comparison with laboratory-based XRD

One of the first applications of the BTX-II was to test interpreted mineralogy logs generated by the HyLogger

scans of drillcore. Infrared reflectance spectra from the core indicated the presence of palygorskite in black shales from both the mineral hole EC157D (Eastern Goldfields Superterrane), and the petroleum well Theia 1 (Canning Basin). Small samples were collected from both drillcores, at locations interpreted to contain significant amounts of palygorskite. The collected samples were analysed using the BTX-II, and mineral phases determined and quantified by RIR analysis using XPowder (Table 4).

To confirm these results, both samples were also subsequently analysed by Mineral Resources Tasmania (MRT) using a laboratory-based Philips X-ray diffractometer system (Cu-anode), which scanned across 2–52° 2θ at a rate of 0.02° per second, with a 0.02° step size (Bottrill and Woolley, 2016). Clay separation and treatment techniques, including heating to 105°C and swelling with glycol, was used for clay mineral identification by MRT (Bottrill and Woolley, 2016). The semi-quantitative RIR analysis of the diffraction patterns by MRT was performed using the software package XPlot (Table 4). Due to the dark colour of the EC157D sample, the C and S content was measured by non-dispersive infrared (NDIR) analysis using a Bruker G4 Icarus analyser, which measured at 21.6% and 15.2% respectively (Bottrill and Woolley, 2016).

Mineral compositions were generally compatible between analysis of diffraction data from the BTX-II and the MRT laboratory-based XRD. The greatest discrepancy between interpreted mineralogy is observed in the EC157D sample, with the identification of pyrite and graphite as indicated from the measured C and S content. The presence of graphite was overlooked due to peak overlap with quartz at

Table 3. CSIRO powdered mineral and rock standards analysed by BTX-II

Reference no.	*Standard*	*Certifying organization*	*Source location*
BCS 368	dolomite	Bureau of Analysed Samples Ltd	Unknown
KGa-2	PX kaolinite	Clay Minerals Society	Warren County, Georgia, US
SAz-1	Ca-montmorillonite	Clay Minerals Society	Apache County, Arizona, US
H-33a	nontronite	American Petroleum Institute	Spokane County, Washington, US
H-49	pyrophyllite	American Petroleum Institute	Robbins County, North Carolina, US
G-2	granite	US Geological Survey	Washington County, Rhode Island, US
SY-2	syenite	Canadian Department of Mines	Hastings County, Ontario, Canada
JB-1	basalt	Geological Survey of Japan	Oshima Subprefecture, Tokyo, Japan
UM-2	ultramafic	Geological Survey of Canada	Kenora District, Ontario, Canada
SARM 39	kimberlite	SA Council of Mineral Technology	Kimberley, North Cape Province, South Africa

Table 4. Comparison of calculated mineral compositions (weight %) using RIR analysis between the BTX-II and MRT laboratory XRD

	EC157D (105.65 m)			*Theia 1 (1610.6 m)*		
Mineral phase	*BTX-II*	*MRT XRD**	*BTX-II Revised*	*BTX-II*	*MRT XRD**	*BTX-II revised*
quartz	19	5–10	15	4	5–10	5
muscovite / mica	61	15–25	49	17	-	-
illite	-	-	-	70	>80	85
pyrite	7	25–35	5	-	-	-
palygorskite	5	-	-	8	-	-
kaolinite	8	15–25	7	-	-	-
graphite	-	15–25	24	-	-	-
halite	-	<2	-	-	-	-
gypsum	-	<2	-	-	-	-
jarosite	-	<2	-	-	-	-
K-feldspar	-	-	-	-	<2	10
montmorillonite	-	-	-	1	-	-

NOTE: * Data from Bottrill and Woolley, 2016

3.34Å, so the BTX-II data was recalculated to incorporate this phase. Observed shifting of the ~10Å clay peaks after the clay treatment methods were applied by MRT is inconsistent with palygorskite (Caillère and Hénin, 1961), and the clay mineral phases were instead identified as muscovite and illite.

Analysis of the samples using the laboratory-based MRT XRD required over 40 minutes for each sample, compared to 20 minutes with the BTX-II. Measured diffraction patterns showed similar X-ray counts from both instruments, although the laboratory-based XRD produced a diffraction pattern with improved noise-to-peak ratio, making peak identification easier. The laboratory-based XRD also used a mechanical goniometer which allowed scanning of lower diffraction angles, which is critical for clay analysis. Differences in calculated proportions of phases are likely partly due to small mineral variations between subsamples, and difference in sample size, as the laboratory-based MRT XRD required significantly more sample for analysis.

Applications of X-ray powder diffractometry

The primary objective of the BTX-II instrument is to enable rapid identification or validation of mineral content of various geological samples. Visual identification of minerals in geological samples can be difficult, particularly for fine-grained, altered, weathered or stained samples. Some related mineral species (e.g. carbonates, garnets) additionally have similar optical properties that make differentiation difficult even when using an optical microscope. The location of the pXRD at the GSWA Perth Core Library allows convenient on-site mineralogical and crystallographic analysis of field and core samples, including drillcore chips and cuttings, to complement current analytical work.

Application of pXRD enables validation of the interpretations of hyperspectral core scans from the GSWA HyLogger-3, and clarification of problematic mineral mixtures. Validation of HyLogger-3 data has a significant value for resource exploration, providing confirmation of interpreted hyperspectral features for use in remote sensing, and aiding in identifying vectors to mineralization (Hancock et al., 2013). The pXRD allows quantitative measurement of crystallographic features, such as Árkai indices (chlorite crystallinity) and Kübler indices (illite crystallinity), useful for characterizing metamorphic grades (Doublier et al., 2010). Quantitative mineralogy of samples is also attainable by using powerful analytical software, providing a more objective assessment of relative mineral compositions (Uvarova et al., 2014; Burkett et al., 2015). Although not exhaustive, the case studies provided below show the potential utility of pXRD to current and future work at GSWA.

Specimens from Greenbushes Li–Cs–Ta pegmatite

The Greenbushes pegmatite is a giant Archean granitic pegmatite deposit, which intruded into the Donnybrook–Bridgetown shear zone of the South West Terrane (Fig. 11; Partington, 1986, 2017; Partington et al., 1995). The Greenbushes pegmatite is an LCT-type (Li–Cs–Ta-rich) rare-element pegmatite deposit (Pollard, 2017), and is the largest hard rock lithium deposit globally, and the site of the longest continually operating mine in Western Australia (Partington, 2017). Mining is currently for the Li-bearing spodumene and Ta-bearing tantalite, but Greenbushes has historically also been mined for tin (Partington, 2017). Several samples of the pegmatite and surrounding country rocks from the pegmatite-wall contacts were collected by GSWA geologists during a visit to the mine site in 2017.

Pegmatite specimen GSWA 201965 contained a brightly coloured red mineral mixture phase visually identified as lepidolite-clay mixture (Fig. 12). To test the validity of the visual identification, small chips from the red phase were collected and analysed by pXRD. The sample was crushed and sieved to a powder (<150 µm) and analysed for approximately 18 minutes (800 s total integration time) using Kapton cell windows. Qualitative analysis of the resulting X-ray diffraction pattern was performed using XPowder. The hand sample was also analysed using the GSWA portable XRF (Thermo Scientific NITON XL3t 955 Ultra), using 120 s integration time (50 kVp, 0.040 mA) and calibrated using the BB1 Bunbury basalt standard (Morris, 2009). Elemental data from the XL3t 955 Ultra is shown in Table 5.

The XRD pattern of GSWA 201965 (Fig. 13) shows that the sample is composed of quartz and various zeolite group minerals, primarily analcime and lesser stilbite-Ca, barrerite, stillwellite-Ce and zeolite. The red colour is attributed to Mn-bearing mineral phases, supported by the detection of Mn in the coupled XRF spectrum (Fig. 14). Due to the unexpected identification of the GSWA 201965 sample as being primarily composed of zeolites, the sample was sent to the CSIRO's Australian Resources Research Centre in Kensington, Perth to confirm the results. The CSIRO analysed the sample using a laboratory-based Bruker D4 Endeavor X-ray powder diffractometer (Co-anode), which scanned across 5–70° 2θ with a collection time of 7 minutes. Qualitative analysis of the resulting X-ray diffraction pattern (Fig. 15) performed using the software XPlot yielded an identical mineralogical interpretation, confirming the results from the BTX-II.

Zeolites associated with lepidolite and tantalum mineralization have previously been described from the Greenbushes pegmatite as pollucite (Partington et al., 1995). Pollucite is a rare Cs-rich zeolite mineral and forms in extremely differentiated zones of LCT-type granitic rare-element pegmatite deposits (Dittrich, 2016; Pollard, 2017). Pollucite is important as the predominant source of Cs produced globally, containing up to 42.6% Cs_2O (Butterman et al., 2005).

Pollucite has a similar crystal structure to analcime, forming a solid-solution series in which Cs is substituted for Na and water (Dittrich, 2016), which results in similar XRD patterns for these minerals including overlap of the most intense peaks. The lack of a large pollucite 321 peak at ~3.66 Å in the GSWA 201965 diffraction pattern (Fig. 13), and the presence of the large analcime 211 peak at ~5.60 Å, indicates that the sample primarily contains analcime. However, the identification of Cs peaks at 4.29 and 4.62 keV in the XRF spectrum (Fig. 14), and the

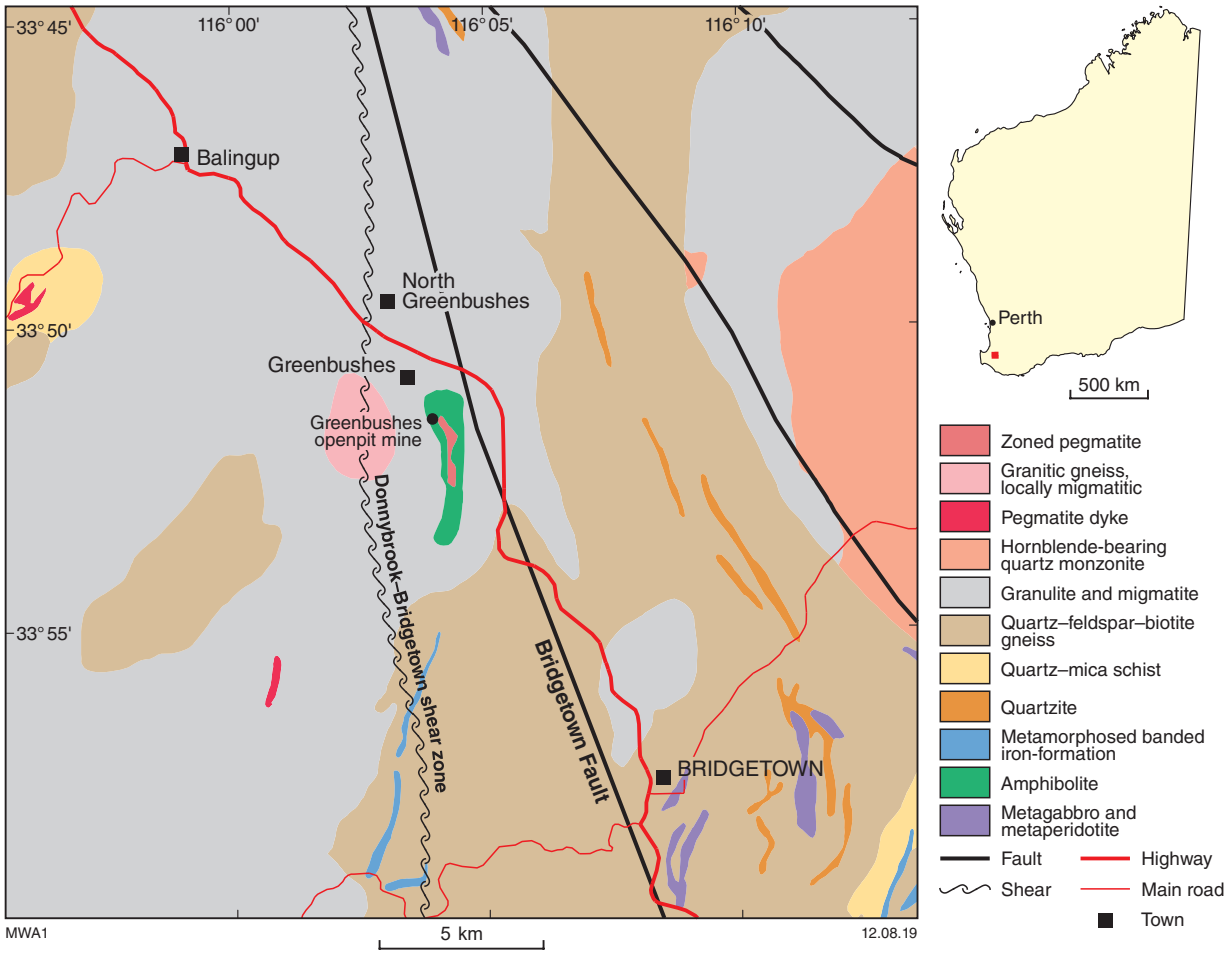

Figure 11. Regional geology of the Greenbushes pegmatite deposit, which intruded into the Western Gneiss Terrane and the Donnybrook–Bridgetown shear zone (approximate location from Partington et al., 1998)

detection of Cs using the Niton XL3t 955 Ultra, confirms the presence of a Cs-rich analcime member of the solid-solution series.

The presence of analcime in GSWA 201965 may represent the crystallization of a highly fractionated melt insufficiently enriched in Cs to exsolve significant pollucite, or pollucite that was leached and analcimized by later hydrothermal fluids (Dittrich, 2016). Alternatively, analcime and the other identified zeolites in GSWA 201965 may have formed during a Cenozoic 'zeolite-carbonate' hydrothermal alteration of the Greenbushes pegmatite district mentioned by Partington et al. (1995), although no further description of this event or its distribution is available. This latter mechanism would require the adsorption of Cs to analcime from hydrothermal fluids, which may be supported by significant adsorption (~1.5%) of As by zeolites, as detected in the associated XRF spectrum and confirmed with pXRF.

Regardless, the misidentification of the primary mineral phase in the sample as lepidolite demonstrates the difficulty of visual identification of minerals in hand specimens. This case study illustrates the capability of pXRD to rectify the problem by enabling quick and accurate identification of minerals in geological samples.

Figure 12. Greenbushes Li deposit pegmatite specimen GSWA 201965, containing a brightly coloured red mineral mixture in a matrix of quartz and spodumene

Table 5. XRF data of the Greenbushes pegmatite samples from the BTX-II and NITON XL3t 955 Ultra

		XL3t 955 Ultra		*BTX-II*	
		Concentration (ppm)		*Observed peak*	
Element	*BB1 standard*	*GSWA 201966*	*GSWA 201965*	*GSWA 201966*	*GSWA 201965*
Ag	7.61	-	9.23	-	-
Al	65 170.34	88 340.55	34 207.06	(a)	(a)
As	8.75	49.25	15 314.88	-	Yes
Au	-	-	-	-	-
Ba	221.83	152.66	197.81	-	-
Bi	-	38.46	226.13	-	-
Ca	63 678.71	10 327.54	19 986.17	Yes	Yes
Cd	-	28.54	20.9	-	-
Ce	188.58	111.26	1011.36	-	-
Cl	255.03	57.83	741.54	(a)	(a)
Co	347.93	-	36.85	(b)	(b)
Cr	326.03	-	115.41	(b)	(b)
Cs	72.31	299.3	3505.63	-	Yes
Cu	128.87	36.8	141.34	-	-
Fe	85 068.05	477.53	497.4	(b)	(b)
Hg	-	12.42	-	-	-
K	6310.49	3330.33	1838.54	Yes	Yes
La	187.21	-	-	-	-
Mg	21 987.22	7507.11	17 463.98	(a)	(a)
Mn	1344.52	5788.13	8605.39	Yes	Yes
Mo	7.31	3.01	5.96	-	-
Nb	6.9	-	7.07	-	-
Ni	138.26	-	330.06	-	-
P	560.71	3491.74	1054.8	(a)	(a)
Pb	-	-	14.03	-	-
Pd	-	4.37	-	-	-
Rb	9.88	454.58	296.38	-	-
S	1110.99	-	1589.18	(a)	(a)
Sb	15.4	62.21	116.27	-	-
Sc	431.49	57.18	131.12	-	-
Se	-	-	17.64	-	-
Si	213 581.97	140 286.23	114 491.71	(a)	(a)
Sn	18.27	115.6	289.68	Yes	(c)
Sr	226.64	210.04	51.42	-	-
Te	32.78	61.19	181.2	-	-
Th	-	21.91	172.8	-	-
Ti	13 710.57	977.06	2557.37	Yes	Yes
U	-	-	-	-	-
V	446.21	-	-	-	-
W	212.81	81.9	-	(b)	(b)
Y	38.4	11.95	-	-	-
Zn	113.95	8.89	41.25	-	-
Zr	149.62	-	-	-	-

NOTES: (a) Element is too light to be detectable by the BTX-II
(b) Background peak present from X-ray source
(c) Peak obscured by other elements

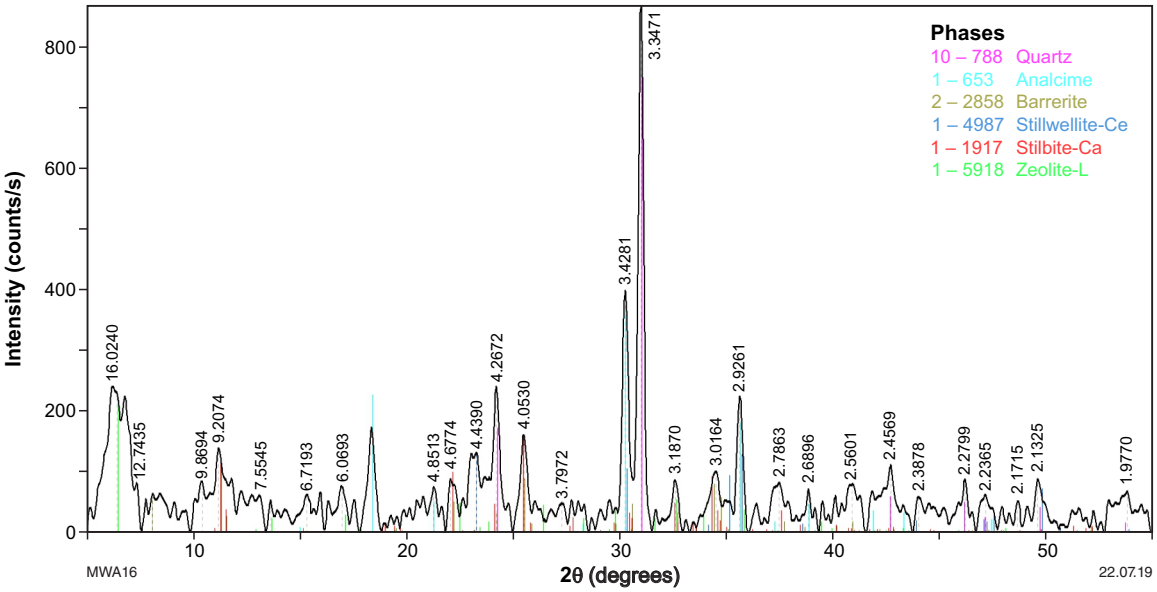

Figure 13. XRD pattern (intensity, cps and 2θ, degrees) of the red mineral mixture in sample GSWA 201965 showing presence of quartz and various zeolite species. GSWA pXRD data analysed using XPowder

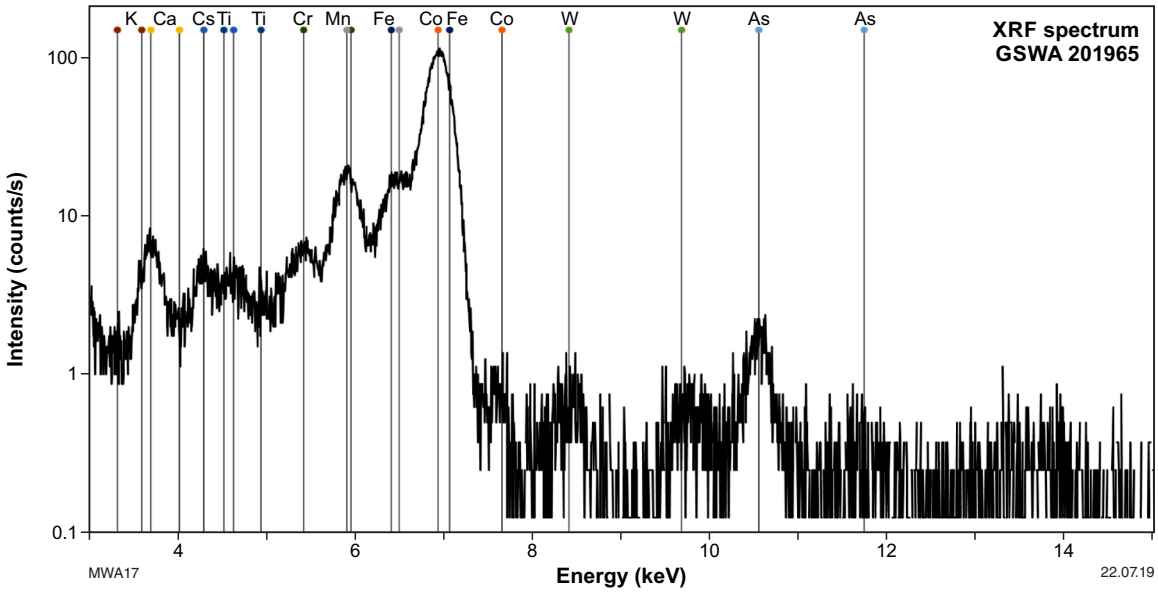

Figure 14. XRF spectrum (intensity, cps and energy, keV) of the red mineral mixture in sample GSWA 201965 analysed using GSWA pXRD and manual data processing

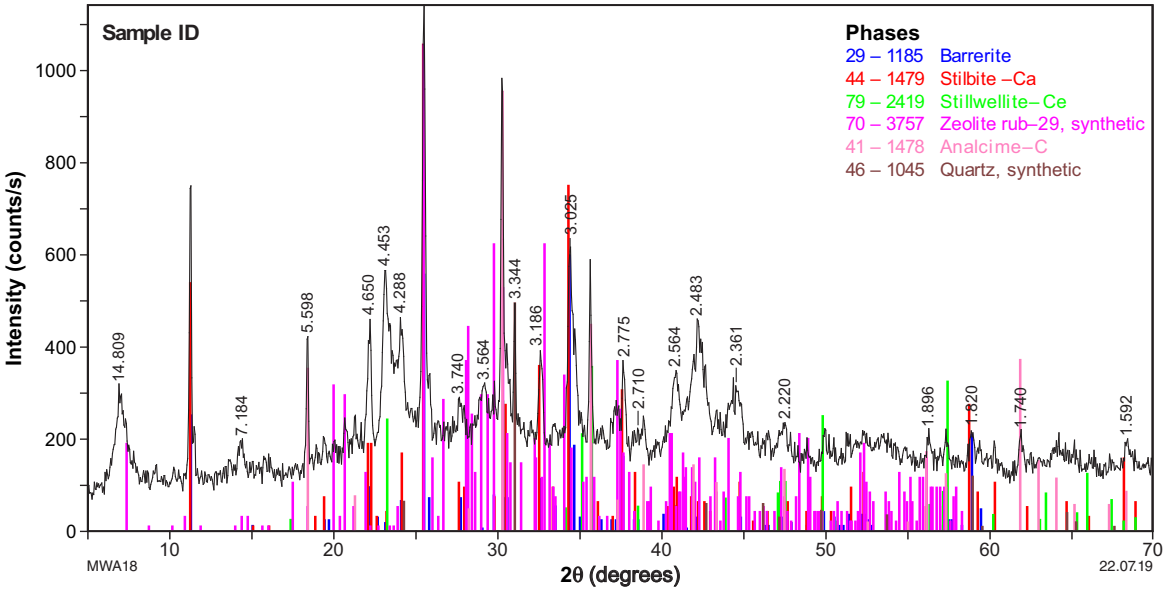

Figure 15. XRD pattern (intensity, counts × 100 in cps and 2θ, degrees) of the red mineral mixture in sample GSWA 201965 showing presence of quartz and various zeolite group minerals. CSIRO Bruker D4 Endeavor data analysed using XPlot

It also provides independent validation of the accuracy of qualitative identifications from the BTX-II, by comparison of results with CSIRO's laboratory-based X-ray powder diffractometer.

Drillcore from the Corybas 1 well

The Corybas 1 gas exploration and appraisal well was drilled in the Yardarino gas field of the northern Perth Basin in 2005 to test the gas production potential of the Early Permian Irwin River Coal Measures and High Cliff Sandstones (Fig. 16; Australian Worldwide Exploration [AWE], 2008). The Corybas 1 diamond drillcore is stored at the GSWA Perth Core Library, and was scanned by the GSWA HyLogger-3 in 2017 as part of ongoing collaborative work between GSWA and industry to assess the carbon sequestration and shale gas potential in the northern Perth Basin (Hancock, 2017). HyLogger core logs are a useful tool for such studies, providing important mineralogical and textural information about the stratigraphy, such as the distribution of clay minerals and carbonate cements that impact on the permeability and porosity of the sedimentary units.

As part of activities to validate the presence of minerals indicated by the interpreted HyLogger-3 data of Corybas 1 well, a small sample chip of sandstone was collected at 2506.13 m depth along the core (Fig. 17), and analysed using pXRD. The sampled section of core consists of fine to very fine-grained sandstone and interbedded coal, with siliceous and locally calcareous cement, occasional argillaceous matrix, and minor traces of mica or pyrite, attributed to the upper portions of the Irwin River Coal Measures (Australian Worldwide Exploration, 2008). Analysis of the HyLogger-3 data using The Spectral Geologist (TSG 7) software indicated the sample is primarily composed of quartz and dickite. The presence of Fe-rich calcite and illitic–muscovite was also indicated by user-interpreted scalars.

The core sample was crushed and sieved to a powder (<150 µm) and analysed for approximately 28 minutes (1250 s total integration time) using Kapton cell windows. Qualitative analysis of the X-ray diffraction pattern using XPowder (Fig. 18) showed that the sample was predominantly composed of quartz, with significant amounts of dickite and calcite. The analysis also showed the presence of minor amounts of muscovite and microcline, and a small fraction of indistinguishable clay minerals (beyond the capabilities of the BTX-II to detect and distinguish). The coupled XRF spectrum indicated the presence of Ca-bearing (calcite) and K-bearing (microcline, muscovite) mineral phases in the sample (Fig. 19). Significant Ti fluorescence was observed, but is likely due to the presence of an accessory phase such as rutile or ilmenite, which was not present in sufficient volume to be detectable in the XRD pattern.

To test the validity of this interpretation, and determine a quantitative composition of the sample, the XRD pattern was analysed by Rietveld refinement using Siroquant. The initial model showed a good fit to the measured pattern, confirming that the identified minerals were sufficient to explain all of the observed diffraction peaks (Fig. 20). A final model with reasonable fit (χ^2 = 4.37, R-Factor = 0.206) was obtained with minor adjustments to crystal dimension, orientation and half-width parameters. The calculated mineral proportions vary from those calculated in XPowder using RIR analysis, but are more consistent with the results from the HyLogger spectral analysis.

This case study took less than an hour between sampling to attaining semiquantitative results, illustrating the ability of pXRD to provide rapid cross-validation of the HyLogger-3

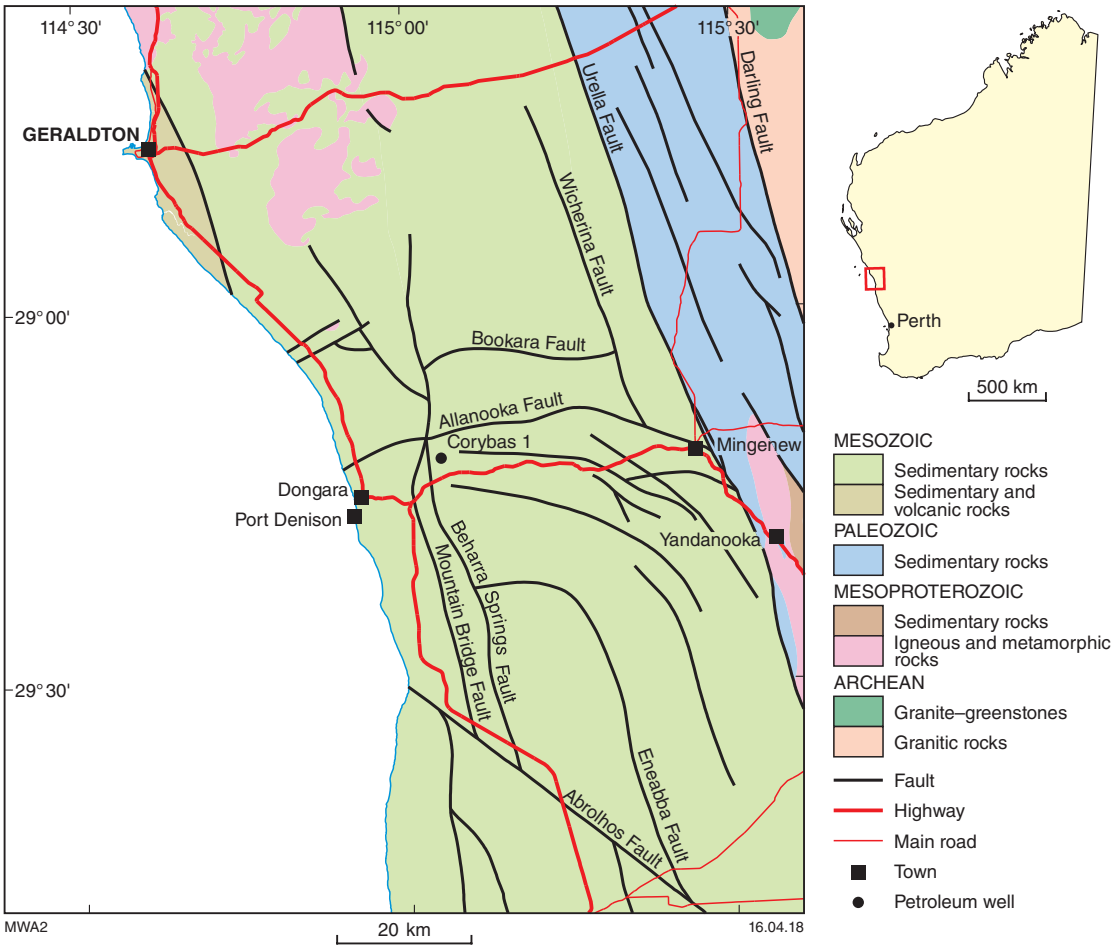

Figure 16. Regional geology and location of the Corybas 1 well in the northern Perth Basin

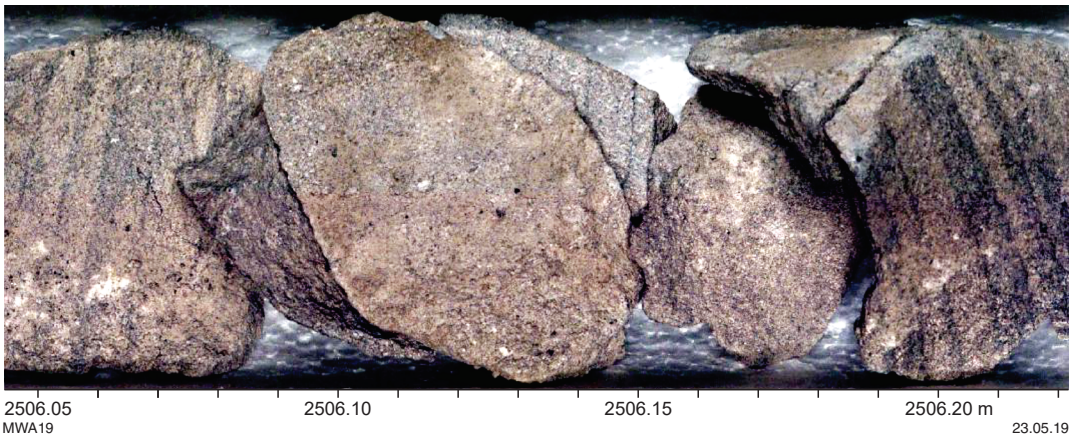

Figure 17. Sandstone core chip sample from 2506.13 m of Corybas 1 well analysed by GSWA pXRD to validate HyLogger data. Image generated by the GSWA HyLogger-3

data. Qualitative results from this XRD analysis confirmed the interpreted mineralogy from HyLogger-3 data, illustrating the accuracy of HyLogger mineralogical core logs. Quantitative results derived from the Rietveld analysis are in agreement with prior petrological studies of nearby core sections (Table 6) using optical microscopy and laboratory-based XRD, demonstrating the potential of pXRD as a supplementary method and to reduce costly additional petrological analysis. Additionally, the ability of the BTX-II to analyse unconsolidated geological samples such as soils, drillcore chips and pulps, in particular may be relevant for petroleum wells and mineral drillholes that lack significant diamond drilled core.

Conclusion

The Olympus BTX-II benchtop XRD analyser significantly adds to the analytical capabilities of GSWA. The pXRD facility allows rapid identification and characterization of various geological samples with minimal preparation, providing support to current GSWA projects and enabling new research methods. Qualitative and quantitative mineralogical analysis of samples is provided by interpretation of generated X-ray data using XPowder and Siroquant software. Application of the pXRD has demonstrated the utility of the instrument to GSWA, allowing the validation of HyLogger-3 hyperspectral core

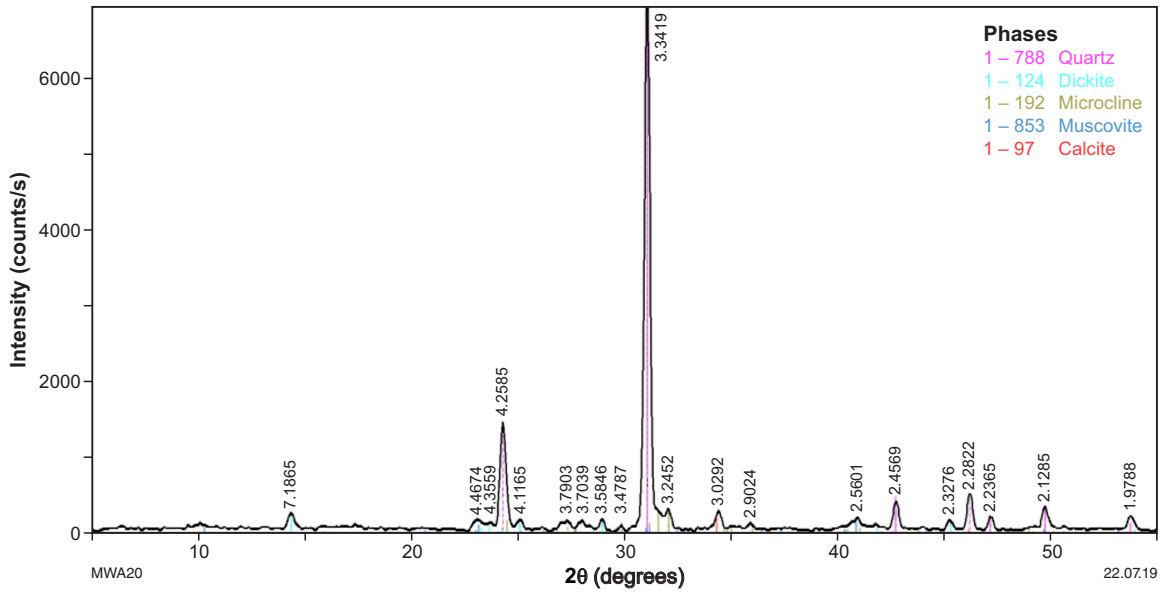

Figure 18. XRD pattern (intensity, cps and 2θ, degrees) of the Corybas 1 well sample showing the presence of quartz, dickite, microcline, muscovite, calcite, and minor undistinguished clays. GSWA pXRD data analysed using XPowder

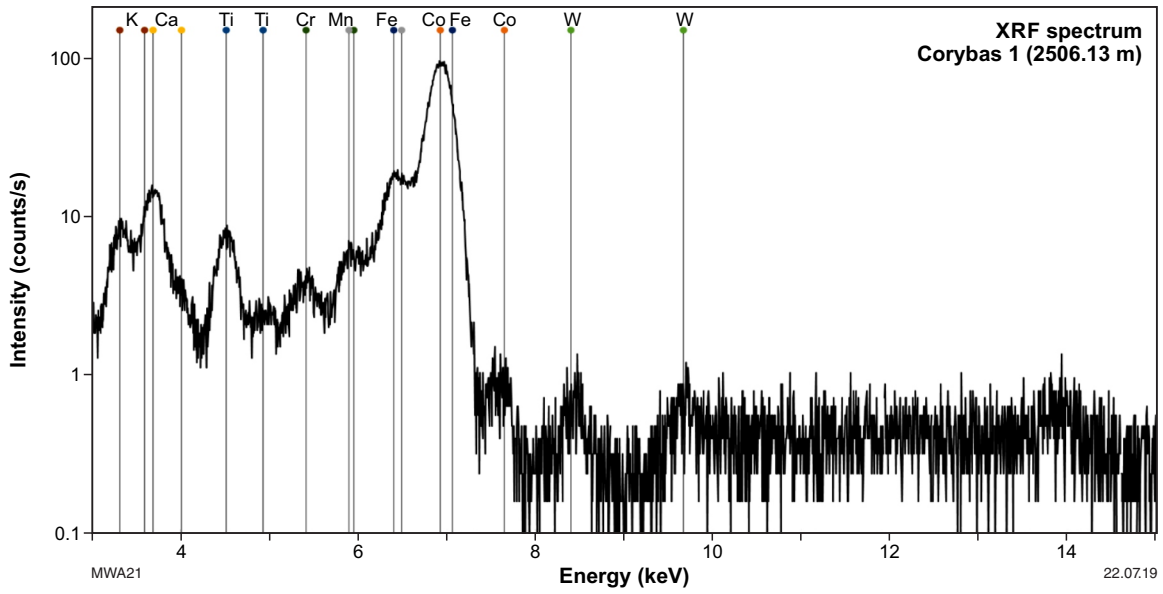

Figure 19. XRF spectrum (intensity, cps and energy, keV) of the Corybas 1 well sample analysed using the GSWA pXRD and manual data processing

logs interpretations, and rapid interpretation of problematic mineral phases.

The pXRD is also capable of providing crystallographic analysis of features including crystallite size and strain, and unit cell parameters. These analytical capabilities can be applied to studies of mineral growth and alteration, support the interpretation and discovery of hyperspectral features, and provide independent validation of other analytical techniques. However, work is required to test the sensitivity and accuracy of the BTX-II for this purpose, which is beyond the scope of this Record. Further work is required to investigate the full analytical capabilities of the coupled XRF detection, including quantifying detection limits of elements, instrumental signature screening and the potential for semiquantitative analysis.

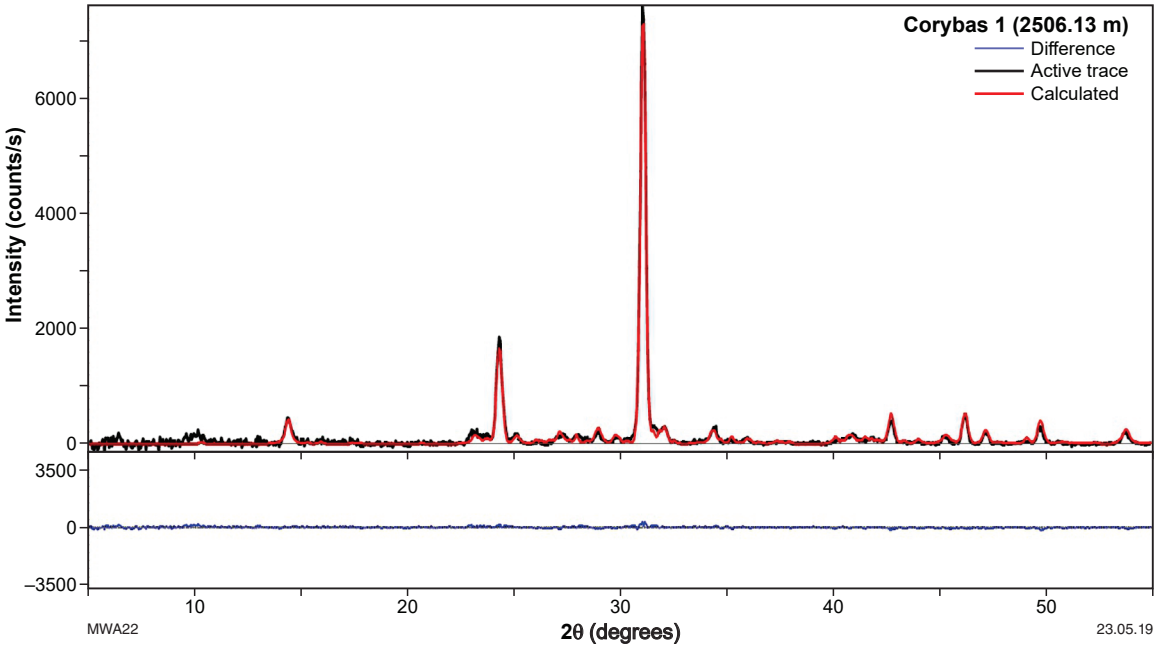

Figure 20. XRD pattern (intensity, cps and 2θ, degrees) of the Corybas 1 well sample analysed using Siroquant, showing the measured pattern (black), modelled pattern (red) and differential (blue)

Table 6. Mineral composition of core samples from the Irwin River Coal Measures in Corybas 1 well analysed using BTX-II and AWE (2008) data

	BTX-II	*Lab XRD**	*Thin section**
Depth	*2506.13 m*	*2507.06 m*	*2509.17 m*
Mineral phase	*Weight (%)*	*Weight (%)*	*Weight (%)*
quartz	67.3	69	66.7
microcline / K-feldspar	14.5	3	13
dickite	10.2	-	9.4
kaolinite	-	3	-
muscovite / mica	4.8	1	-
smectite / illite	-	17	4.7
calcite	3.3	3	-
siderite	-	1	-
dolomite	-	1	-
pyrite	-	1	-
lithic fragments	-	-	4.7

NOTE: * Data from AWE (2008)

References

Alagarsamy, P 2016, Structure analysis tools — Lecture 3: Powder diffraction, in Characterization of Materials: National Programme on Technology Enhanced Learning (NPTEL) — Phase II, <https://nptel.ac.in/courses/115103030/module2/lec3/1.html>.

Árkai, P 1991, Chlorite crystallinity: an empirical approach and correlation with illite crystallinity, coal rank and mineral facies as exemplified by Palaeozoic and Mesozoic rocks of northeast Hungary: Journal of Metamorphic Geology, v. 9, no. 6, p. 723–734.

Australian Worldwide Exploration 2008, Corybas 1 basic and interpretive well completion report; Geological Survey of Western Australia, Statutory petroleum exploration report, W20969 A5.

Barnes, P, Jacques, S and Vickers, M 2016, Diffraction Theory II: From Structure Factors to Diffraction Intensities — Powder Diffraction, *in* Advance Certificate in Powder Diffraction on the Web: Course Material *edited by* JK Cockcroft: Birbeck College, London, UK, <http://pd.chem.ucl.ac.uk/pdnn/diff2/kinemat2.htm>.

Bish, DL, Blake, D, Vaniman, D, Sarrazin, P, Bristow, T, Achilles, C, Dera, P, Chipera, S, Crisp, J, Downs, RT, Farmer, J, Gailhanou, M, Ming, D, Morookian, JM, Morris, R, Morrison, S, Rampe, E, Treiman, A and Yen, A 2014, The first X-ray diffraction measurements on Mars: International Union of Crystallography Journal, v. 1, no. 6, p. 514–522, doi:10.1107/S2052252514021150.

Bish, DL and Howard, SA 1988, Quantitative phase analysis using the Rietveld method: Journal of Applied Crystallography, v. 21, no. 2, p. 86–91.

Bish, DL, Reynolds, RC and Post, JE 1989, Sample preparation for X-ray diffraction: Reviews in Mineralogy and Geochemistry, v. 20, p. 73–99.

Blake, D, Vaniman, D, Anderson, R, Bish, D, Chipera, S, Chemtob, S, Crisp, J, Des-Marais, DJ, Downs, R, Farmer, J, Gailhanou, M, Ming, D, Morris, D, Stolper, E Sarrazin, P, Treiman, A and Yen, A 2009, The CheMin mineralogical instrument on the Mars Science Laboratory Mission: Lunar and Planetary Science Conference, v. 40.

Bottrill, RS and Woolley, RN 2016, Mineralogical/Petrology Report LJN2015/140; Mineral Resources Tasmania.

Brindley, GW 1961, Experimental methods, *in* The X-ray identification and crystal structures of clay minerals (2nd ed.) *edited by* G Brown: Mineralogical Society, Clay Minerals Group, London, UK, p. 1–50.

Burkett, DA, Graham, IT and Ward, CR 2015, The application of portable X-ray diffraction to quantitative mineralogical analysis of hydrothermal systems: The Canadian Mineralogist, v. 53, no. 3, p. 429–454.

Butterman, WC, Brooks, WE and Reese Jr, RG 2005, Mineral commodity profiles: cesium, in Mineral Commodity Profiles 2004-1432, United States Geological Survey, Reston, Virginia, USA, <https://www.usgs.gov/centers/nmic/commodity-statistics-and-information>.

Caillère, S and Hénin, S 1961, Palygorskite, *in* The X-ray identification and crystal structures of clay minerals (2nd ed.) *edited by* G Brown: Mineralogical Society, Clay Minerals Group, London, UK, p. 343–353.

Chipera, SJ and Bish, DL 2013, Fitting full X-ray diffraction patterns for quantitative analysis: A method for readily quantifying crystalline and disordered phases: Advances in Materials Physics and Chemistry, v. 3, no. 1, p. 47–53.

Chung, FH 1974, Quantitative interpretation of X-ray diffraction patterns of mixtures, I. Matrix-flushing method for quantitative multicomponent analysis: Journal of Applied Crystallography v. 7, no. 6, p. 519–525.

Cullity, BD 1956, Elements of X Ray Diffraction: Addison-Wesley Publishing Company, Addison-Wesley series in metallurgy and materials, p. 1–514.

Dittrich, T 2016, Meso- to Neoarchean lithium-cesium-tantalum-(LCT-) pegmatites (Western Australia, Zimbabwe) and a genetic model for the formation of massive pollucite mineralisations; Freiberg University of Mining and Technology, Frieberg, PhD thesis, p. 1–355.

Doublier, MP, Roache, A and Potel, S 2010, Application of SWIR spectroscopy in very low-grade metamorphic environments: A comparison with XRD methods: Geological Survey of Western Australia, Record 2010/7, 61p.

Fischer instrumentation (GB) Ltd nd, X-Ray Fluorescence, <www.fischergb.co.uk/en/united-kingdom/knowledge/methods/material-testing/x-ray-fluorescence2>.

Geological Survey of Western Australia 2016, Geological survey work program for 2016–17 and beyond: Geological Survey of Western Australia, Record 2016/1, 168p.

Hancock, EA 2017, Hylogger-3 National Virtual Core Library: Hylogger studies on petroleum core (poster), Petroleum Open Day 2017: Geological Survey of Western Australia, 15 September 2017.

Hancock, EA, Green, AA, Huntington, JF, Schodlok, MC and Whitbourn, LB 2013, HyLogger-3: Implications of adding thermal-infrared sensing: Geological Survey of Western Australia, Record 2013/3, 24p.

Hillier, S 2000, Accurate quantitative analysis of clay and other minerals in sandstones by XRD: Comparison of a Rietveld and a reference intensity ratio (RIR) method and the importance of sample preparation: Clay Minerals, v. 35, p. 291–302.

Jenkins, R and Snyder, RL 1996, Introduction to X-ray Powder Diffraction: Chemical Analysis, in A Series of Monographs on Analytical Chemistry and its Applications edited by JD Winefordner: John Wiley & Sons, Inc., New York, US, v. 138, 403p.

Klein, C and Dutrow, B 2007, Manual of Mineral Science: Wiley, Hoboken, US, 675p.

Martin, JD 2012, XPowder User Guide, viewed 9 April 2019, <www.xpowder.com/download/xpowder.pdf>.

Mitra, S 1996, Fundamentals of Optical, Spectroscopic and X-ray Mineralogy (2nd edition): New Age International Ltd, New Delhi, India, 336p.

Moore, DM and Reynolds, RC 1989, X-ray diffraction and the identification and analysis of clay minerals: Oxford University Press, New York, p. 1–332.

Morris, PA 2009, Field-portable X-ray fluorescence analysis and its application in GSWA: Geological Survey of Western Australia, Record 2009/7, 23p.

Olympus NDT 2014, BTX II X-ray Diffraction Analyzer User's Manual: DMTA-10031-01EN [U8023504]: Waltham, US, viewed 28 March 2018, <www.olympus-ims.com/en/.downloads/download/?file=285215333&fl=en_US>.

Partington, GA 1986, The tectonic controls on the intrusion of specialized pegmatites in the Greenbushes pegmatite district, Western Australia: Australian Bureau of Mineral Resources, Record 1986/10, p. 53–54.

Partington, GA 2017, Greenbushes tin, tantalum and lithium deposit, *in* Australian Ore Deposits *edited by* GN Phillips: Australasian Institute of Mining and Metallurgy, Monograph 32, p. 153–158.

Partington, GA, McNaughton, NJ and Williams, IS 1995, A review of the geology, mineralization, and geochronology of the Greenbushes Pegmatite, Western Australia: Economic Geology, v. 90, p. 616–635.

Pollard, PJ 2017, Australian rare element granitic pegmatites, *in* Australian Ore Deposits *edited by* GN Phillips: Australasian Institute of Mining and Metallurgy, Monograph 32, p. 67–74.

Sarrazin, P, Chipera, S, Bish, D, Blake, D and Vaniman, D 2005, Vibrating sample holder for XRD analysis with minimal sample preparation: Advances in X-ray Analysis, v. 48, p. 156–164.

Sientronics Pty Ltd 2006, Siroquant Version 3.0 Technical and Clays Manual; Sientronics Pty Ltd, Belconnen, Australian Capital Territory, viewed 9 April 2019, <www.siroquant.com>.

Sientronics Pty Ltd 2007, Siroquant Version 3.0 User Manual; Sientronics Pty Ltd, Belconnen, Australian Capital Territory, viewed 9 April 2019, <www.siroquant.com>.

Uvarova, YA, Cleverley, JS, Verrall, M and Baensch, A 2014, Coupled XRF and XRD analyses for rapid and low-cost characterization of geological materials in the mineral exploration and mining industry: Explore, v. 162, p. 4–14.

Veqter Ltd 2019, X-ray diffraction, <www.veqter.co.uk/residual-stress-measurement/x-ray-diffraction>.

Ward, CR and Gómez-Fernández, F 2003, Quantitative mineralogical analysis of Spanish roofing slates using the Rietveld method and X-ray powder diffraction data: Journal of Geochemical Exploration, v. 15, no. 6, p. 1051–1062.

Wilson, AJ 1949, X-ray Optics: The diffraction of X-rays by finite and imperfect crystals: Methuen, p. 1–127.

Appendix

CSIRO powdered mineral and rock standards analysed by BTX-II

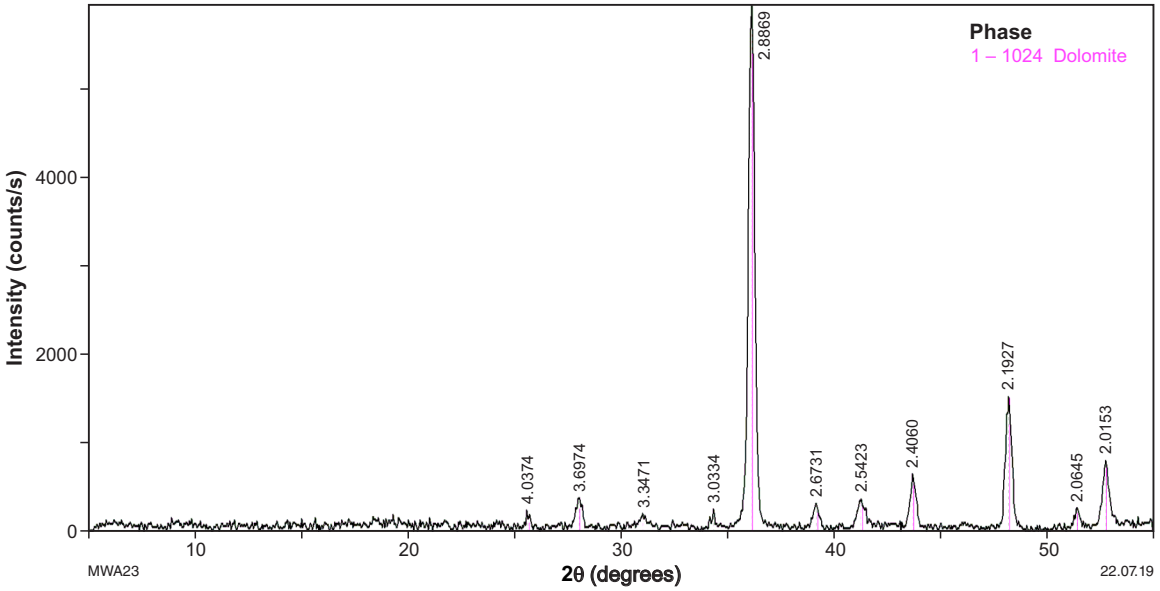

Figure A1. XRD pattern (intensity, c.p.s. and 2θ, degrees) of the powdered mineral standard BCS 368, containing pure dolomite. GSWA pXRD data analysed using XPowder

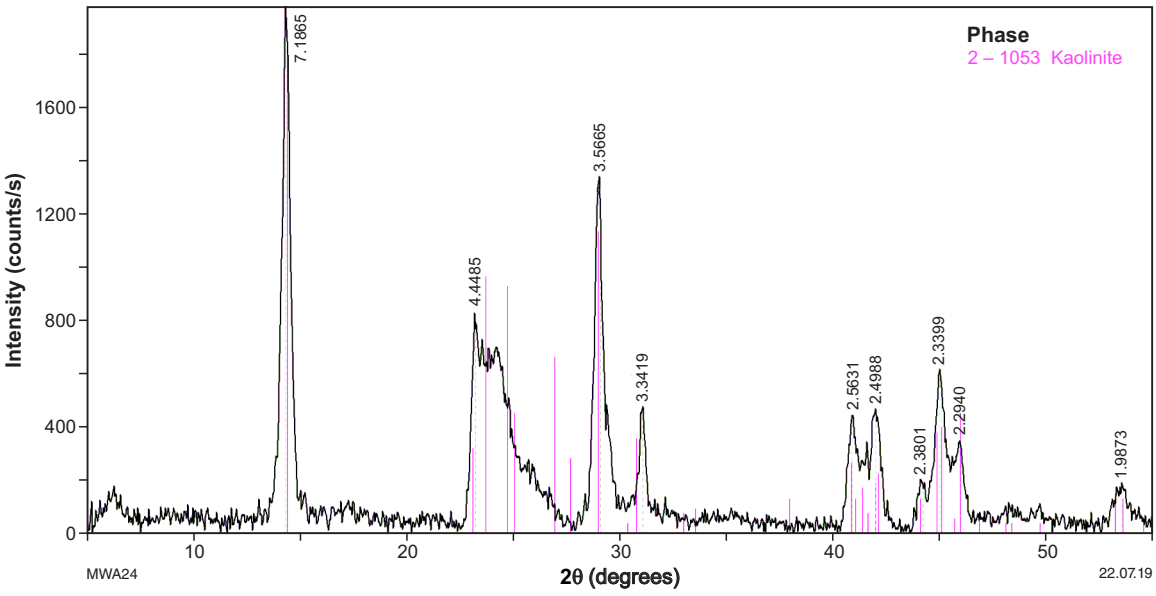

Figure A2. XRD pattern (intensity, cps and 2θ, degrees) of the powdered mineral standard KGa-2, containing pure, poorly crystalline kaolinite. GSWA pXRD data analysed using XPowder

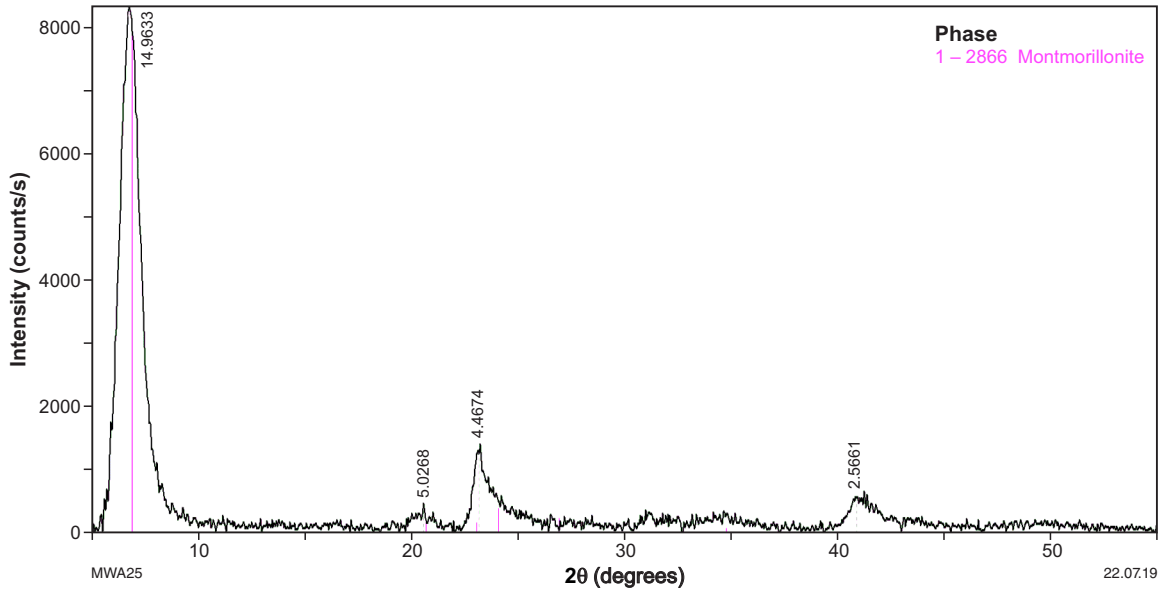

Figure A3. XRD pattern (intensity, cps. and 2θ, degrees) of the powdered mineral standard SAz-1, containing pure Ca-montmorillonite. GSWA pXRD data analysed using XPowder

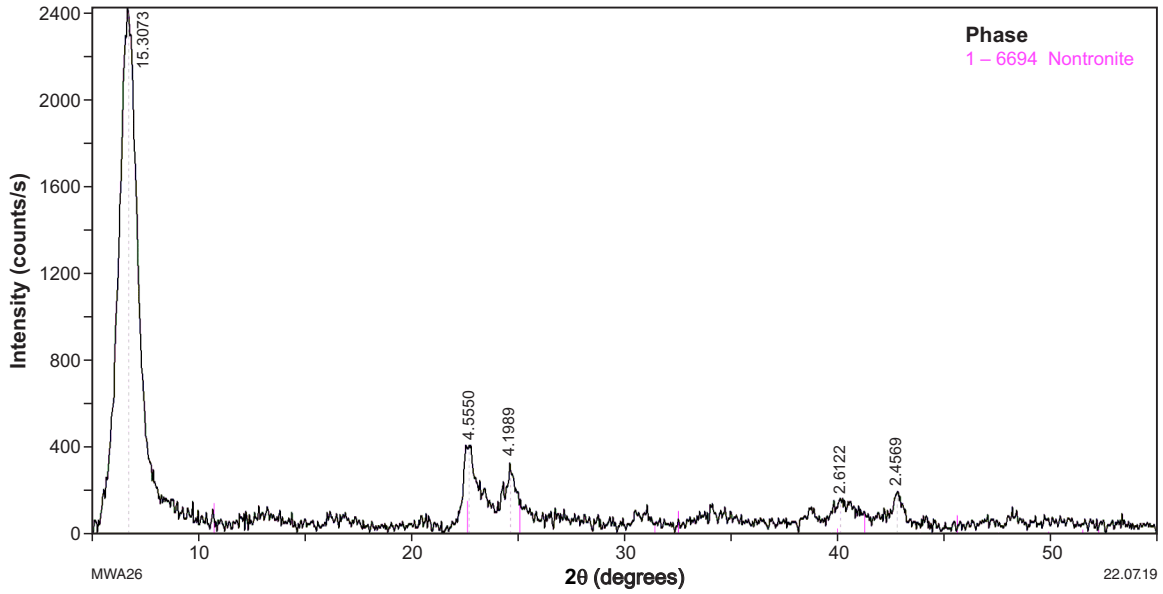

Figure A4. XRD pattern (intensity, cps and 2θ, degrees) of the powdered mineral standard H-33a, containing pure nontronite. GSWA pXRD data analysed using XPowder

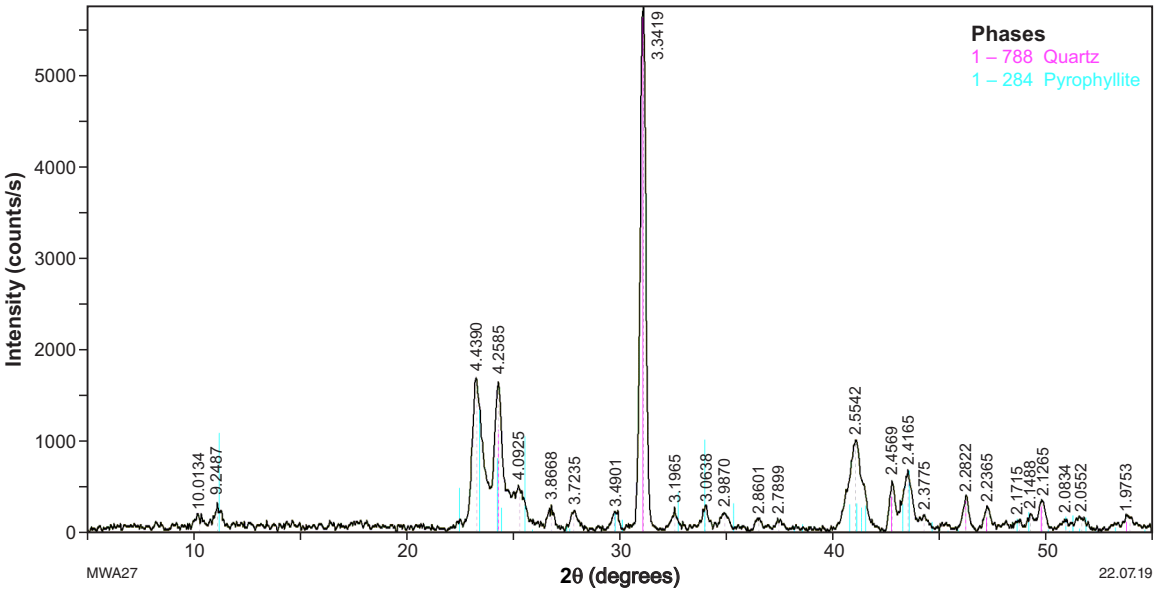

Figure A5. XRD pattern (intensity, cps and 2θ, degrees) of the powdered mineral standard H-49, containing pyrophyllite and quartz. GSWA pXRD data analysed using XPowder

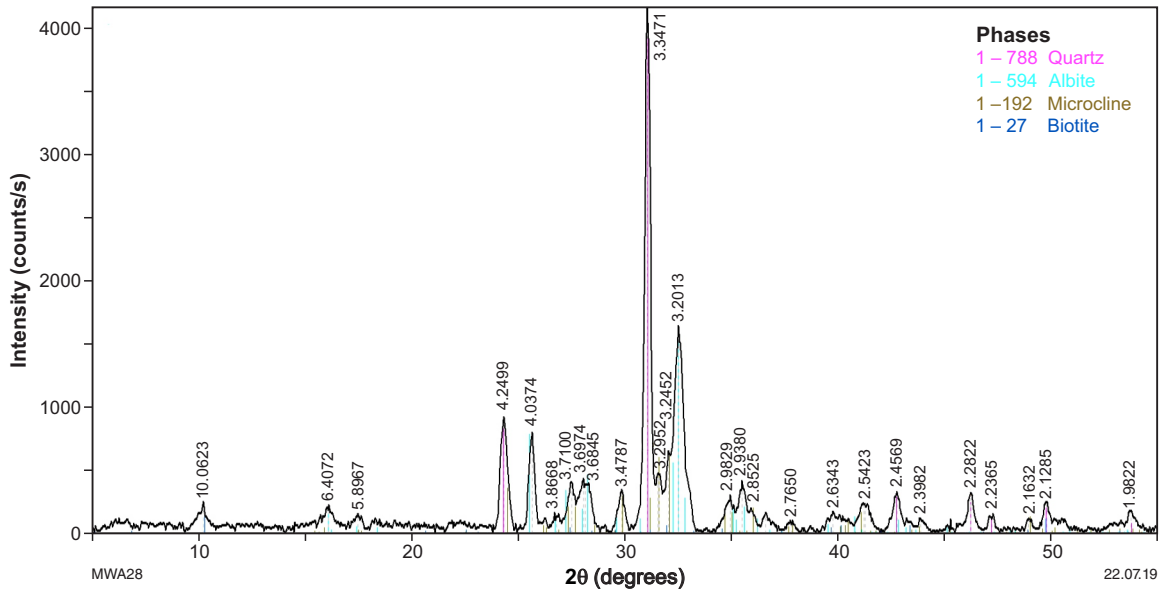

Figure A6. XRD pattern (intensity, cps and 2θ, degrees) of the powdered rock standard G-2, containing multiple phases identified as quartz, albite, microcline and biotite. GSWA pXRD data analysed using XPowder

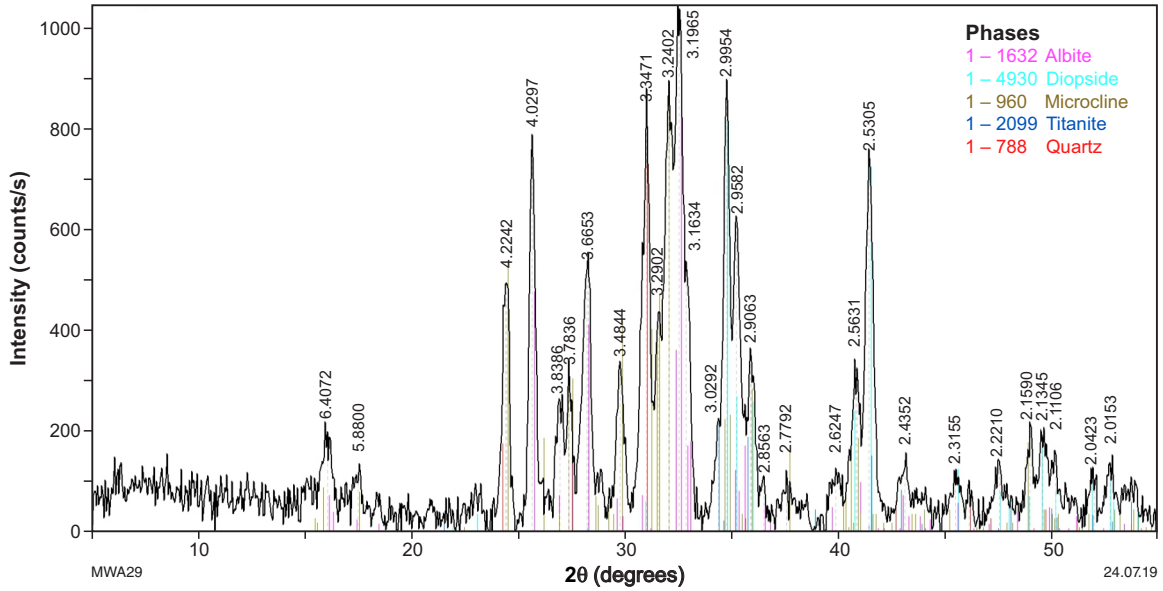

Figure A7. XRD pattern (intensity, cps and 2θ, degrees) of the powdered rock standard SY-2, containing multiple phases identified as albite, diopside, microcline, titanite and quartz. GSWA pXRD data analysed using XPowder

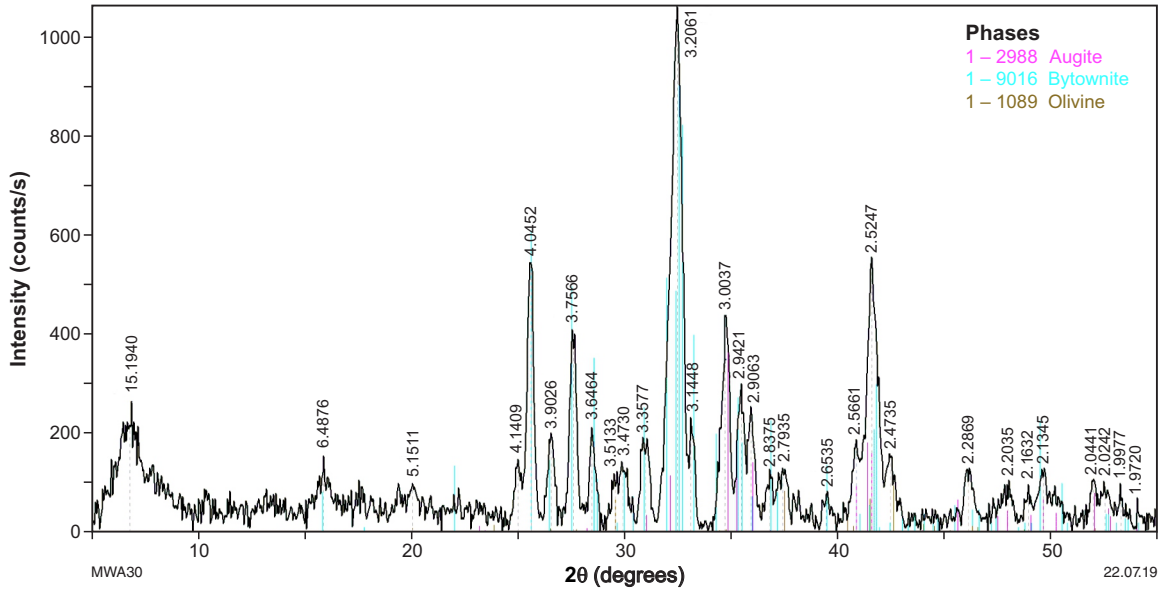

Figure A8. XRD pattern (intensity, cps and 2θ, degrees) of the powdered rock standard JB-1, containing multiple phases identified as augite, bytownite and olivine. Note the possible Kapton peak at ~16Å. GSWA pXRD data analysed using XPowder

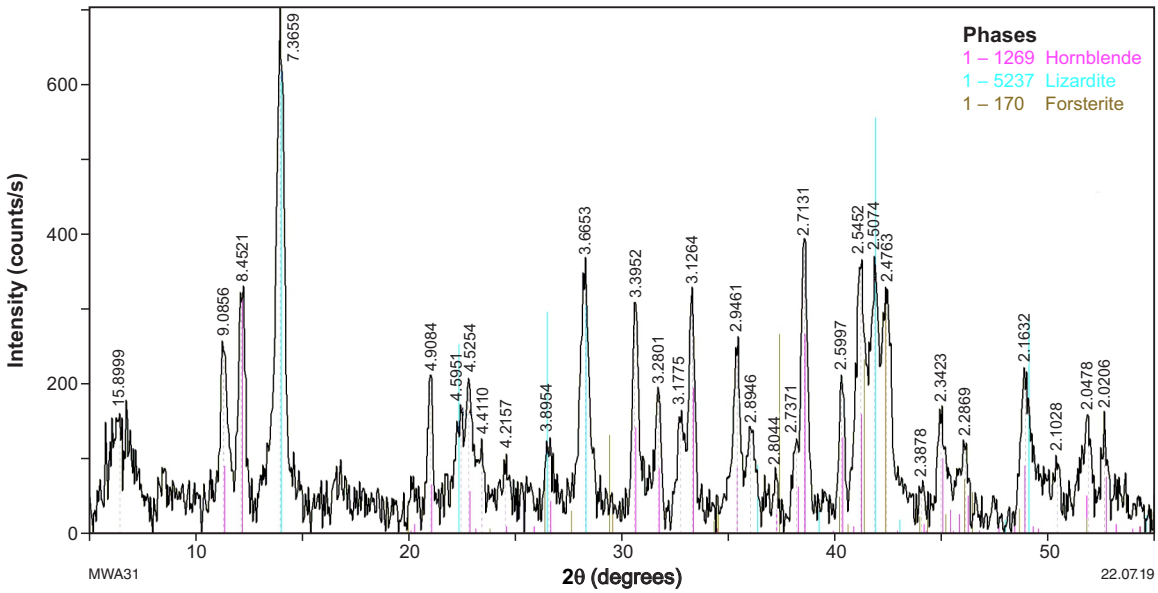

Figure A9. XRD pattern (intensity, cps and 2θ, degrees) of the powdered rock standard UM-2, containing multiple phases identified as hornblende, lizardite and forsterite. Note the possible Kapton peak at ~16Å. GSWA pXRD data analysed using XPowder

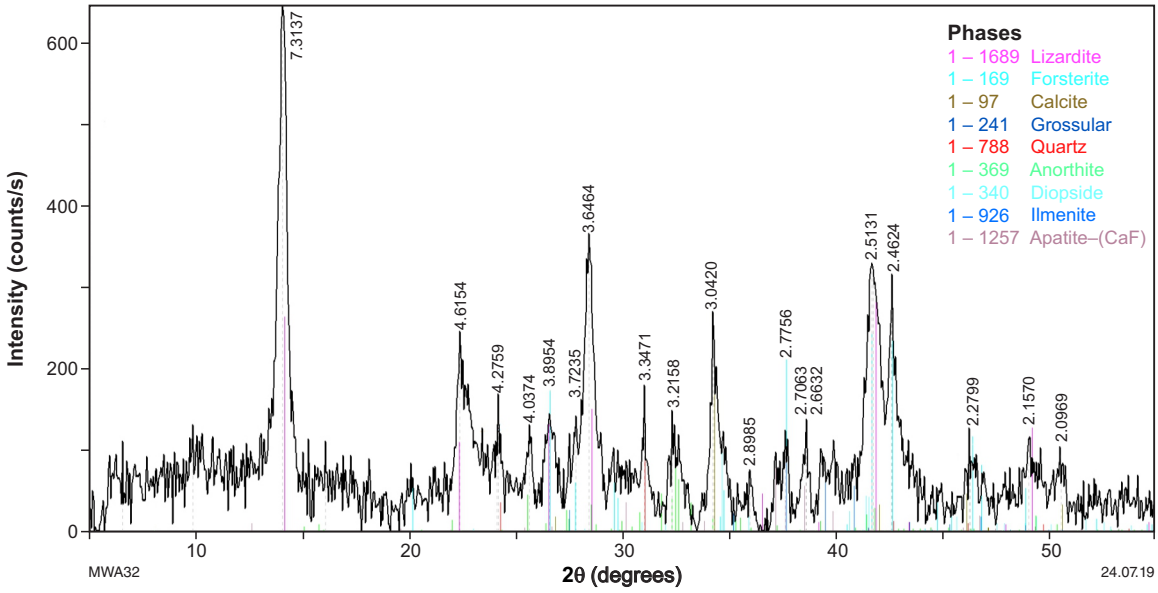

Figure A10. XRD pattern (intensity, cps and 2θ, degrees) of the powdered rock standard SARM 39, containing multiple phases identified as lizardite, forsterite, calcite, grossular, quartz, anorthite, diopside, ilmenite and apatite. GSWA pXRD data analysed using XPowder

RECORD 2019/9

APPLICATION OF RAPID BENCHTOP X-RAY POWDER DIFFRACTOMETRY FOR IDENTIFICATION AND CHARACTERIZATION OF MINERAL PHASES IN GEOLOGICAL MATERIALS

Wawryk and Hancock

This Record is published in digital format (PDF) and is available as a free download from the DMIRS website at <www.dmp.wa.gov.au/GSWApublications>.

Further details of geoscience products can be obtained by contacting:

Information Centre
Department of Mines, Industry Regulation and Safety
100 Plain Street
EAST PERTH WESTERN AUSTRALIA 6004
Phone: +61 8 9222 3459 Fax: +61 8 9222 3444
www.dmp.wa.gov.au/GSWApublications